


2012

# CFD study on aerodynamic effects of a rear wing/ spoiler on a passenger vehicle

Mustafa Cakir  
*Santa Clara University*

Follow this and additional works at: [http://scholarcommons.scu.edu/mech\\_mstr](http://scholarcommons.scu.edu/mech_mstr)

 Part of the [Aerodynamics and Fluid Mechanics Commons](#), and the [Mechanical Engineering Commons](#)

---

## Recommended Citation

Cakir, Mustafa, "CFD study on aerodynamic effects of a rear wing/spoiler on a passenger vehicle" (2012). *Mechanical Engineering Masters Theses*. Paper 1.

This Thesis is brought to you for free and open access by the Student Scholarship at Scholar Commons. It has been accepted for inclusion in Mechanical Engineering Masters Theses by an authorized administrator of Scholar Commons. For more information, please contact [rsccroggin@scu.edu](mailto:rsccroggin@scu.edu).

SANTA CLARA UNIVERSITY

Department of Mechanical Engineering

December 2012

I HEREBY RECOMMEND THAT THE THESIS PREPARED UNDER  
MY SUPERVISOR BY

**Mustafa Cakir**

ENTITLED  
**CFD STUDY ON AERODYNAMIC EFFECTS OF A REAR WING/SPOILER ON  
A PASSENGER VEHICLE**

BE ACCEPTED IN PARTIAL FULFILLMENT OF  
THE REQUIREMENTS FOR THE DEGREE  
OF  
**MASTER OF SCIENCE IN MECHANICAL ENGINEERING**

---

Thesis Advisor

---

Chairman of Department

Department of Mechanical Engineering

December 2012

SANTA CLARA UNIVERSITY

Department of Mechanical Engineering

December 2012

I HEREBY RECOMMEND THAT THE THESIS PREPARED UNDER  
MY SUPERVISOR BY

**Mustafa Cakir**

ENTITLED  
**CFD STUDY ON AERODYNAMIC EFFECTS OF A REAR WING/SPOILER ON  
A PASSENGER VEHICLE**

BE ACCEPTED IN PARTIAL FULFILLMENT OF  
THE REQUIREMENTS FOR THE DEGREE  
OF  
**MASTER OF SCIENCE IN MECHANICAL ENGINEERING**

---

Thesis Advisor

---

Thesis Reader

---

Chairman of Department

Department of Mechanical Engineering

December 2012

**CFD STUDY ON AERODYNAMIC EFFECTS OF A REAR WING/SPOILER ON  
A PASSENGER VEHICLE**

By  
Mustafa Cakir

MASTER THESIS

Submitted in Partial Fulfillment of the Requirements  
For the Degree of Master of Science  
In Mechanical Engineering  
In the School of Engineering at  
Santa Clara University, December 2012

Santa Clara, California

## TABLE OF CONTENTS

<b>LIST OF FIGURES .....</b>	<b>iii</b>
<b>LIST OF TABLES .....</b>	<b>v</b>
<b>ABSTRACT.....</b>	<b>vi</b>
<b>1 AUTOMOBILE AERODYNAMICS.....</b>	<b>1</b>
<b>1.1 WHAT IS AERODYNAMICS?.....</b>	<b>1</b>
<b>1.2 SCOPE OF AERODYNAMICS .....</b>	<b>2</b>
<b>1.3 EXTERNAL FLOW PHENOMENA OF AUTOMOBILE .....</b>	<b>3</b>
<b>1.4 FACTORS CONTRIBUTING TO FLOW FIELD AROUND VEHICLE .....</b>	<b>5</b>
1.4.1 BOUNDARY LAYER .....	5
1.4.2 FLOW SEPARATION .....	5
1.4.3 FRICTION DRAG .....	7
1.4.4 PRESSURE DRAG .....	7
<b>1.5 FORCES AND MOMENT ON VEHICLE .....</b>	<b>8</b>
<b>2 CFD (COMPUTATIONAL FLUID DYNAMICS).....</b>	<b>10</b>
<b>2.1 WHAT IS CFD? .....</b>	<b>10</b>
<b>2.2 ADVANTAGES OF COMPUTATIONAL FLUID DYNAMICS .....</b>	<b>12</b>
<b>2.3 NUMERICAL METHOD .....</b>	<b>13</b>
2.3.1 PRE-PROCESSOR.....	14
2.3.2 NUMERICAL SOLVER .....	16
2.3.3 POST PROCESSOR.....	18
<b>3 VEHICLE AND THE SPOILER .....</b>	<b>18</b>
<b>3.1 INTRODUCTION TO SPOILER .....</b>	<b>18</b>
<b>3.2 GENERIC MODELS.....</b>	<b>19</b>
3.2.1 VEHICLE GENERIC MODELS AND DIMENSIONS .....	19
3.2.2 SPOILER GENERIC MODELS AND DIMENSIONS .....	21
<b>4 NUMERICAL SIMULATION .....</b>	<b>22</b>
<b>4.1 CAD MODELS.....</b>	<b>22</b>
<b>4.2 VIRTUAL WIND TUNNEL AND VEHICLE ORIENTATION .....</b>	<b>25</b>
<b>4.3 MESH GENERAION .....</b>	<b>30</b>

4.3.1	MESH SIZING AND INFLATION .....	30
4.4	VALIDATION PROCEDURE .....	36
4.5	SOLVER SETTINGS .....	37
5	SIMULATION RESULTS .....	40
5.1	SIMULATION RESULTS OF CASE #1, CASE #2 AND CASE #3 .....	40
5.2	SIMULATION RESULTS OF BENCHMARK #1, BENCHMARK #2 AND BENCHMARK #3 .....	48
5.2.1	BENCHMARK #1: EXAMINE GRID CONVERGENCE .....	49
5.2.2	BENCHMARK #2: EXAMINE GRID CONVERGENCE .....	52
5.2.3	BENCHMARK #3: EXAMINE MODEL UNCERTAINTIES .....	55
6	CONCLUSION .....	58
7	FUTURE WORKS.....	60
	LIST OF REFERENCE .....	61

## LIST OF FIGURES

<b>Figure 1.1</b> Fuel energy usage at urban driving .....	2
<b>Figure 1.2</b> Fuel energy usage at highway driving .....	3
<b>Figure 1.3</b> Streamline of external flows around a stationary vehicle.....	4
<b>Figure 1.4</b> Flow Separation at the rear of vehicle .....	6
<b>Figure 1.5</b> Flow Separation at the rear of vehicle with rear spoiler.....	7
<b>Figure 1.6</b> Forces On Vehicle Body .....	8
<b>Figure 2.1</b> The different disciplines contained within computational fluid dynamics [2] .....	11
<b>Figure 2.2</b> The three basic approaches to solve problems in fluid dynamics and heat transfer. [2] .....	12
<b>Figure 2.3</b> The inter-connectivity functions of the three main elements within a CFD analysis framework. [2] .....	14
<b>Figure 2.4</b> An overview of the solution procedure [2] .....	17
<b>Figure 3.1</b> Dimensions of the generic vehicle model [side-view].....	20
<b>Figure 3.2</b> Dimensions of the generic vehicle model [back-view] .....	20
<b>Figure 3.3</b> Generic model and dimensions of first spoiler.....	21
<b>Figure 3.4</b> Generic model and dimensions of second spoiler .....	22
<b>Figure 4.1</b> Vehicle 3D CAD model.....	23
<b>Figure 4.2</b> First spoiler 3D CAD model .....	23
<b>Figure 4.3</b> Second spoiler 3D CAD model .....	24
<b>Figure 4.4</b> Assembly 3D CAD model of vehicle and first spoiler.....	24
<b>Figure 4.5</b> Assembly 3D CAD model of vehicle and second spoiler .....	25
<b>Figure 4.6</b> Virtual wind tunnel and the vehicle orientation .....	26
<b>Figure 4.7</b> Virtual wind tunnel surface labeling for automatic appropriate boundary conditions. a) Velocity-inlet, b) Symmetry, c) symmetry-top, d) symmetry-side, e) pressure-outlet, f) wall.....	29
<b>Figure 4.8</b> Mesh generation with standard settings.....	30
<b>Figure 4.9</b> Mesh generation with modified sizing settings. ....	31
<b>Figure 4.10</b> Mesh generation with the inflation layers .....	32

<b>Figure 4.11</b> Virtual car-box orientation.....	33
<b>Figure 4.12</b> The final mesh.....	34
<b>Figure 5.1</b> The scaled residuals convergence history for case #1 .....	41
<b>Figure 5.2</b> The scaled residuals convergence history for case #2 .....	41
<b>Figure 5.3</b> The scaled residuals convergence history for case #3 .....	42
<b>Figure 5.4</b> Drag coefficient ( $C_D$ ) convergence histories of case #1 and case #2.....	43
<b>Figure 5.5</b> Velocity distribution of flow in the symmetry plane for case #1 ( <i>maximum velocity: 39.59 m/s</i> ).....	44
<b>Figure 5.6</b> Velocity distribution of flow in the symmetry plane for case #2 ( <i>maximum velocity: 41.45 m/s</i> ).....	45
<b>Figure 5.7</b> Velocity distribution of flow in the symmetry plane for case #3 ( <i>maximum velocity: 39.54 m/s</i> ).....	45
<b>Figure 5.8</b> Velocity streamlines of flow in the symmetry plane for case #1.....	46
<b>Figure 5.9</b> Velocity streamlines of flow in the symmetry plane for case #2.....	46
<b>Figure 5.10</b> Velocity vectors of flow in the symmetry plane for case #1 .....	47
<b>Figure 5.11</b> Velocity vectors of flow in the symmetry plane for case #2 .....	48
<b>Figure 5.12</b> The coarse mesh that used in benchmark #1 .....	49
<b>Figure 5.13</b> Scaled residuals convergence history of benchmark #1 .....	50
<b>Figure 5.14</b> $C_L$ convergence history of benchmark #1.....	50
<b>Figure 5.15</b> $C_D$ convergence history of benchmark #1 .....	51
<b>Figure 5.16</b> The medium mesh that used in benchmark #2 .....	52
<b>Figure 5.17</b> Scaled residuals convergence history of benchmark #2.....	53
<b>Figure 5.18</b> $C_D$ convergence history of benchmark #2 .....	53
<b>Figure 5.19</b> $C_L$ convergence history of benchmark #2.....	54
<b>Figure 5.20</b> Scaled residuals convergence history of benchmark #3.....	56
<b>Figure 5.21</b> $C_L$ convergence history of benchmark #3.....	56
<b>Figure 5.22</b> $C_D$ convergence history of benchmark #3 .....	57



## LIST OF TABLES

<b>Table 4-a Mesh sizing parameters.....</b>	<b>35</b>
<b>Table 4-b Solver settings .....</b>	<b>38</b>
<b>Table 4-c Viscous model and turbulence model settings.....</b>	<b>39</b>
<b>Table 4-d Boundary condition settings .....</b>	<b>39</b>
<b>Table 5-a Drag and lift coefficients for 3 cases .....</b>	<b>44</b>
<b>Table 5-b Drag and lift coefficients for 3 cases + benchmark #1 .....</b>	<b>51</b>
<b>Table 5-c Drag and lift coefficients for 3 cases + benchmark #1 + benchmark #2... </b>	<b>54</b>
<b>Table 5-d Drag and lift coefficients for 3 cases + benchmark #1 + benchmark #2 + benchmark #3 .....</b>	<b>58</b>

## ABSTRACT

Aerodynamic characteristics of a racing car are of significant interest in reducing car-racing accidents due to wind loading and in reducing the fuel consumption. At the present, modified car racing becomes more popular around the world. Sports cars are most commonly seen with spoilers, such as Ford Mustang, Subaru Impreza, and Chevrolet Corvette. Even though these vehicles typically have a more rigid chassis and a stiffer suspension to aid in high-speed maneuverability, a spoiler can still be beneficial.

One of the design goals of a spoiler is to reduce drag and increase fuel efficiency. Many vehicles have a fairly steep downward angle going from the rear edge of the roof down to the trunk or tail of the car. Air flowing across the roof tumbles over this edge at higher speeds, causing flow separation. The flow of air becomes turbulent and a low-pressure zone is created, thus increases drag. Adding a spoiler at the very rear of the vehicle makes the air slice longer, gentler slope from the roof to the spoiler, which helps to reduce the flow separation. Reducing flow separation decreases drag, which increases fuel economy; it also helps keep the rear window clear because the air flows smoothly through the rear window.

The limitations of conventional wind tunnel experiment and rapid developments in computer hardware, considerable efforts have been invested in the last decade to study vehicle aerodynamics computationally. This thesis will present a numerical simulation of flow around racing car with spoiler positioned at the rear end using commercial fluid dynamic software ANSYS FLUENT<sup>®</sup>. The thesis will focus on CFD-based lift and drag prediction on the car body after the spoiler is mounted at the rear edge of the vehicle. A 3D computer model of 4-door sedan car (which will be designed with commercial software SolidWorks<sup>®</sup>) will be used as the base model. Different spoilers, in different locations will be positioned at the rear end of vehicle and the simulation will be run in order to determine the aerodynamic effects of spoiler.

# **1 AUTOMOBILE AERODYNAMICS**

## **1.1 WHAT IS AERODYNAMICS?**

Aerodynamics is the way objects move through air. The rules of aerodynamics explain how an airplane is able to fly. Anything that moves through air is affected by aerodynamics, from a rocket blasting off, to a kite flying. Since they are surrounded by air, even cars are affected by aerodynamics [15]. “Aerodynamics” is a branch of fluid dynamics concerned with studying the motion of air, particularly when it interacts with a moving object. Aerodynamics is also a subfield gas dynamics, with much theory shared with fluid dynamics. Aerodynamics has often used synonymously with gas dynamics, with the difference being that gas dynamics applies to compressible flows. Understanding the motion of air (often called a flow field) around an object enables the calculation of forces and moments acting on the object. Typical properties calculated for a flow field include velocity, pressure, density and temperature as a function of position and time. By defining a control volume around the flow field, equations for the conservation of mass, momentum, and energy can be defined and used to solve for the properties. The use of aerodynamics through mathematical analysis, empirical approximation and wind tunnel experimentation form the scientific basis.

Aerodynamics can be divided into two sub-categories as external and internal aerodynamics. External aerodynamics is basically the study of flow around solid objects of various shapes. Evaluating the lift and drag on an airplane, the flow of air over a wind turbine blade or the shock waves that form in front of the nose of a rocket are examples of external aerodynamics. Internal aerodynamics on the other hand is the study of flow through passages in solid objects. For instance, internal aerodynamics encompasses the study of the airflow through a jet engine or through an air conditioning pipe. This thesis concentrates more on the external category of the aerodynamics related to vehicle with the domain geometry and grid display, vector plots, line and shaded contour plots, 2D and 3D surface plots, particle tracking and lastly XY plots and graphs of results.

## 1.2 SCOPE OF AERODYNAMICS

The regulation of green house gases to control global warming and rapidly increasing fuel prices have given tremendous pressure on the design engineers to enhance the current designs of the automobile using minimal changes in the shapes. To fulfill the above requirements, design engineers have been using the concepts of aerodynamics to enhance the efficiency of automobiles [16].

Although aerodynamics depends on so many factors, this thesis concentrates on external devices, which affect the flow around the automobile body to reduce the resistance of the vehicle in normal working conditions.

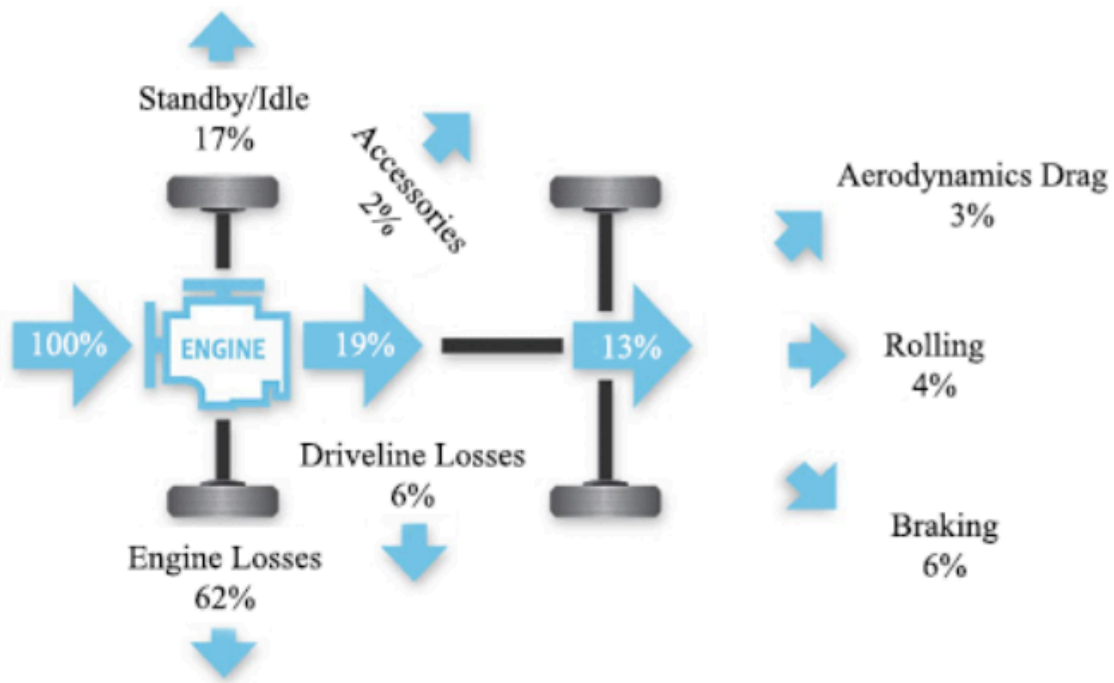


*Figure 1.1 Fuel energy usage at urban driving*

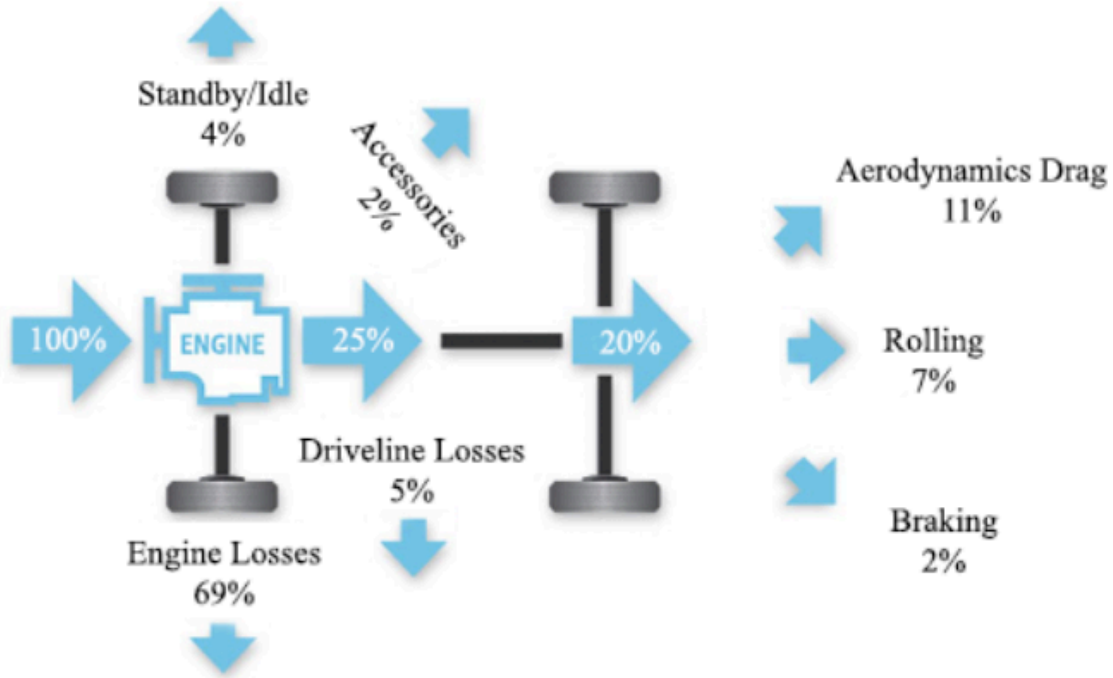


**Figure 1.2 Fuel energy usage at highway driving**

*Figure 1.1* and *Figure 1.2* show the description of the fuel energy used in a modern vehicle at urban driving and highway driving respectively. The shape of the vehicle uses about 3% of fuel to overcome the resistance in urban driving, while it takes 11% of fuel for the highway driving. This considerable high value of fuel usage in highway driving attracts several design engineers to enhance the aerodynamics of the vehicle using minimal design changes. This brings the idea of using external devices, which could be attached to the present vehicle without changing the body. This thesis is based on the design, developments and numeral calculation of the effects of external device, which will be spoiler that mounted at the rear side of the vehicle to make the present vehicles more aerodynamically attractive.

### 1.3 EXTERNAL FLOW PHENOMENA OF AUTOMOBILE

*Figure 1.3* shows the streamline of an external flow around a stationary vehicle. When the vehicle is moving at a certain velocity, the viscous effects in the fluid are restricted to a thin layer called boundary layer. Outside the boundary layer is the inviscid

flow. This fluid flow imposes pressure force on the boundary layer. When the air reaches the rear part of the vehicle, the fluid gets detached. Within the boundary layer, the movement of the fluid is totally governed by the viscous effects of the fluid.

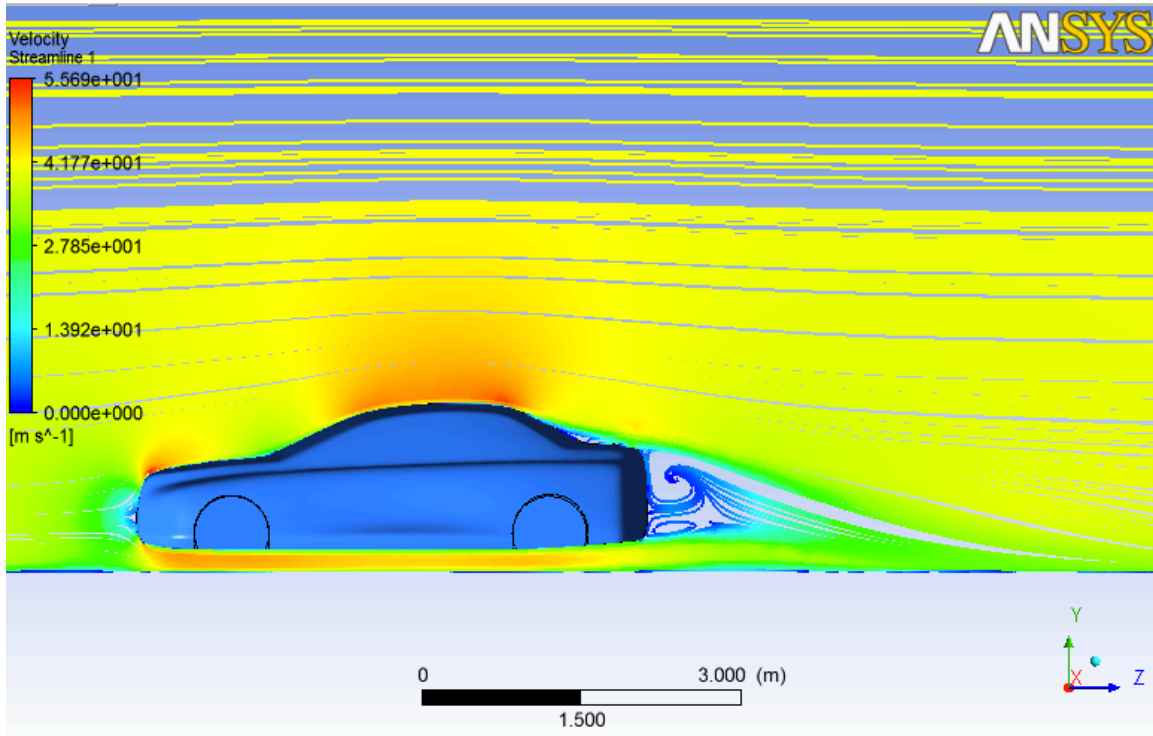


**Figure 1.3** Streamline of external flows around a stationary vehicle

The Reynolds number is dependent on the characteristic length of the vehicle, the kinematic viscosity and the speed of the vehicle. The fluid moving around the vehicle is dependent on the shape of the vehicle and the Reynolds number. There is another important phenomenon, which affects the flow of the car and the performance of the vehicle. This phenomenon is commonly known as ‘Wake’ of the vehicle. When the air moving over the vehicle is separated at the rear end, it leaves a large low-pressure turbulent region behind the vehicle known as the wake. This wake contributes to the formation of pressure drag, which is eventually reduces the vehicle performance.

## **1.4 FACTORS CONTRIBUTING TO FLOW FIELD AROUND VEHICLE**

The major factors, which affect the flow field around the vehicle, are the boundary layers, separation of flow field, friction drag and lastly the pressure drag.

### **1.4.1 BOUNDARY LAYER**

Ludwig Prandtl first defined the aerodynamic boundary layer in a paper presented on August 12, 1904 at the third International Congress of Mathematicians in Heidelberg, Germany. This allows aerodynamicists to simplify the equations of fluid flow by dividing the flow field into two areas: one inside the boundary layer and the one outside the boundary layer. In this boundary layer around the vehicle, the viscosity is dominant and it plays a major role in drag of the vehicle. The viscosity is neglected in the fluid regions outside this boundary layer since it does not have significant effect on the solution. In the design of the body shape, the boundary layer is given high attention to reduce drag [9, 15, 16]. There are two reasons why designers consider the boundary layer as a major factor in aerodynamic drag. The first is that the boundary layer adds to the effective thickness of the body, through the displacement thickness, hence increasing the pressure drag. The second reason is that the shear forces at the surface of the vehicle causes skin friction drag, which arises from the friction of the fluid against the skin of the object that is moving through it [9].

### **1.4.2 FLOW SEPARATION**

During the flow over the surface of the vehicle, there are some points when the change in velocity comes to stall and the fluid starts flowing in reverse direction. This phenomenon is called ‘Separation’ of the fluid flow. This usually occurs at the rear part of the vehicle. This separation is mostly dependent on the pressure distribution, which is imposed by the outer layer of the flow [15]. This separation causes the flow to change its behavior behind the vehicle and thereby affects the flow field around the vehicle. This phenomenon is the major factor to be considered while studying the wake of the vehicle.

Flow separation is bad because it leads to a larger wake and less pressure on the rear surface which reducing pressure recovery. To avoid bad flow separation, the transitions of the airflows from roof to the rear window need to be smoothed [15]. The bad separation also can create more drag. The aerodynamic will be more effective if the flows working in clean air (laminar flow). By improving the aerodynamic of the car can reduce the boundary layer thickness thus avoids worst flow separations.

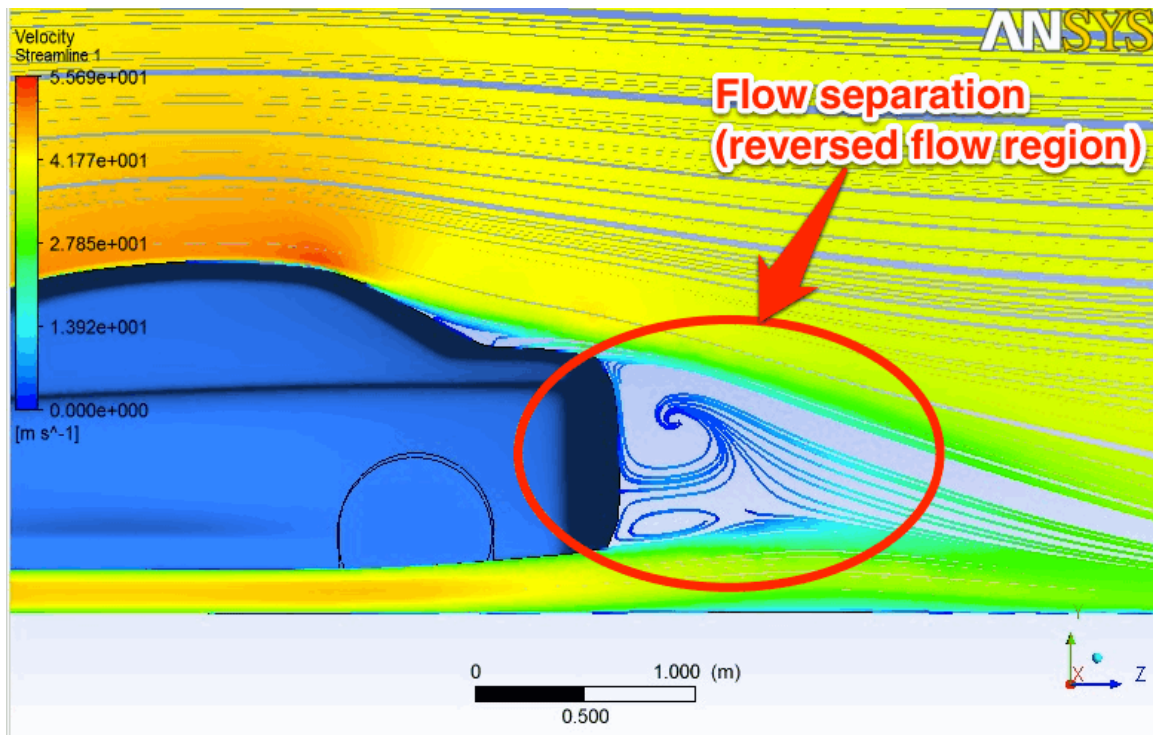


**Figure 1.4** Flow Separation at the rear of vehicle



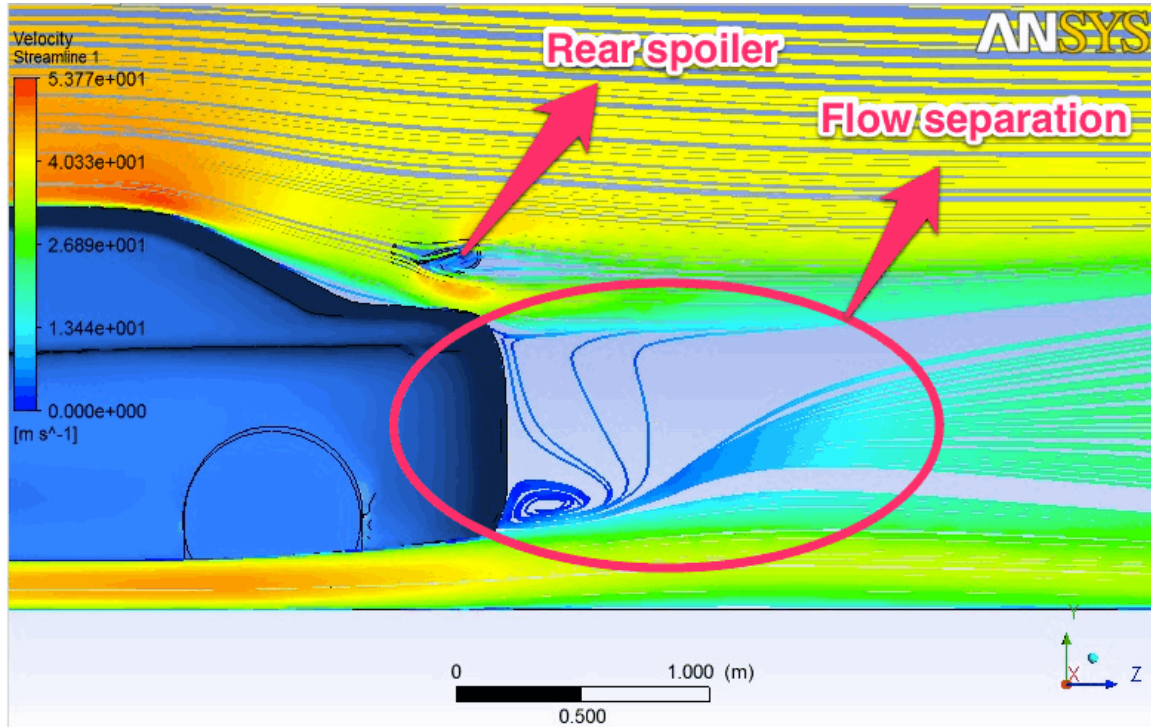


**Figure 1.5 Flow Separation at the rear of vehicle with rear spoiler**

### 1.4.3 FRICTION DRAG

Every material or wall has a distinct friction, which resists the flow of fluids. Due to molecular friction, a stress acts on every surface of the vehicle. The integration of the corresponding force component in the free stream direction leads to a friction drag. If the separation does not occur, then friction drag is one of the main reasons to cause overall drag.

### 1.4.4 PRESSURE DRAG

Behind the vehicles, there is a steep pressure gradient, which leads to the separation of the flow separation in viscous flow. The front part of the flow field shows high-pressure value, whereas on the rear part flow separates leading to a high suction in the area. As we integrate the force component created by such high change in pressure, the resultant is called as 'Pressure Drag'. This factor is affected by the height of the vehicle as well as the separation of the flow field.

## 1.5 FORCES AND MOMENT ON VEHICLE

When the vehicle is moving at a considerable speed, there are several forces are applied to vehicle in different directions. *Figure 1.5* shows the details sketch view of the various forces acting on the vehicle body. As shown in the free body diagram below, there are six forces acting on the vehicle:

- Rolling Resistance
- Drag
- Lift
- Gravity
- Normal
- Motor

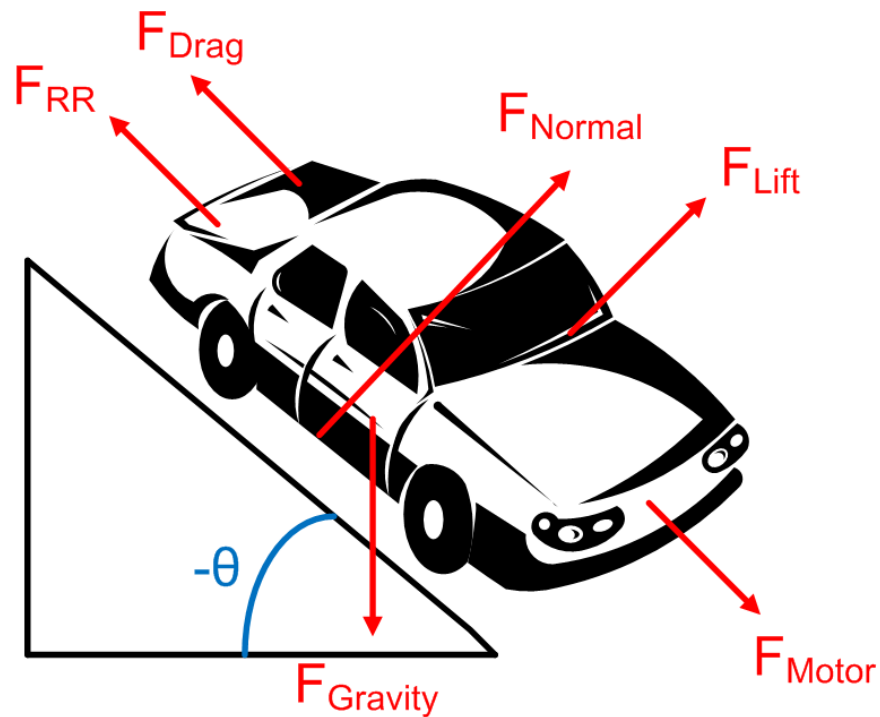


*Figure 1.6* Forces On Vehicle Body

Rolling resistance force is due the tires deforming when contacting the surface of a road and varies depending on the surface being driven on. The normal force is the force exerted by the road on the vehicle's tires. Because the vehicle is not moving up or down

(relative to the road), the magnitude of the normal forces equals the magnitude of the force due to gravity in the direction normal to the road.

Lift force acting on the vehicle body vertically. This force causes the vehicle to get lifted in air as applied in the positive direction, whereas it can result in excessive wheel down force if it is applied in negative direction. Engineers try to keep this value to a required limit to avoid excess down force or lift. The formula usually used to define this force is written as:

$$C_L = \frac{L}{\frac{1}{2}\rho V^2 A} \quad [1.1]$$

Where;

- $L$  : Lift force
- $C_L$  : Lift coefficient
- $A$  : Frontal area of the vehicle
- $\rho$  : Air density
- $V$  : Vehicle velocity

Aerodynamic drag force is the force acting on the vehicle body resisting its forward motion. This force is an important force to be considered while designing the external body of the vehicle, since it covers about 65% of the total force acting on the complete body. The Aerodynamic drag force is calculated by the following formula:

$$C_D = \frac{D}{\frac{1}{2}\rho V^2 A} \quad [1.2]$$

Where;

- $D$  : Drag force
- $C_D$  : Drag coefficient
- $A$  : Frontal area of the vehicle
- $\rho$  : Air density
- $V$  : Vehicle velocity

## 2 CFD (COMPUTATIONAL FLUID DYNAMICS)

### 2.1 WHAT IS CFD?

According to Oleg Zikanov [3] CFD can be defined as:

“CFD (Computational fluid dynamics) is a set of numerical methods applied to obtain approximate solution of problems of fluid dynamics and heat transfer.”

According to this definition, CFD is not a science by itself but a way to apply methods of one discipline (numerical analysis) to another (heat and mass transfer). In retrospect, it is integrating not only the disciplines of fluid mechanics with mathematics but also with computer science as illustrated in *Figure 2.1*. The physical characteristics of the fluid motion can usually be described through fundamental mathematical equations, usually in partial differential form, which govern a process of interest and are often called governing equations in CFD. Jiyuan Tu, Guan Heng Yeoh and Chaoqun Liu [2] has discussed how to solve mathematical equations with using CFD:

“In order to solve mathematical equations, computer scientists convert them by using high-level computer programming languages into computer programs or software packages. The computational part simply means the study of the fluid flow through numerical simulations, which involves employing computer programs or software packages performed on high-speed digital computers to attain the numerical solutions. Another question arises "Do we actually require the expertise of three specific people from each discipline -fluids engineering, mathematics, and computer science- to come together for the development of CFD programs or even to conduct CFD simulations?" The answer is obviously no, and more likely it is expected that this field demands a person who will proficiently obtain some subsets of the knowledge from each discipline.”

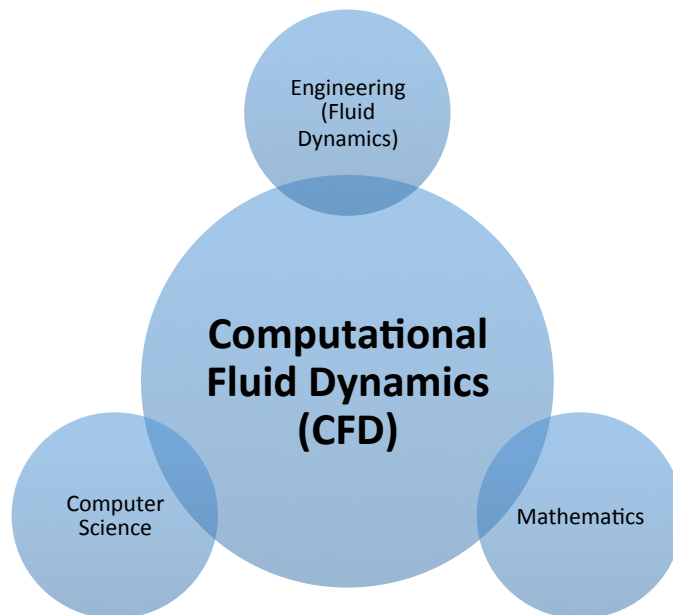


**Figure 2.1** The different disciplines contained within computational fluid dynamics

[2]

CFD has also become one of the three basic methods or approaches that can be employed to solve problems in fluid dynamics and heat transfer. As demonstrated in **Figure 2.2**, each approach is strongly interlinked and does not lie in isolation.

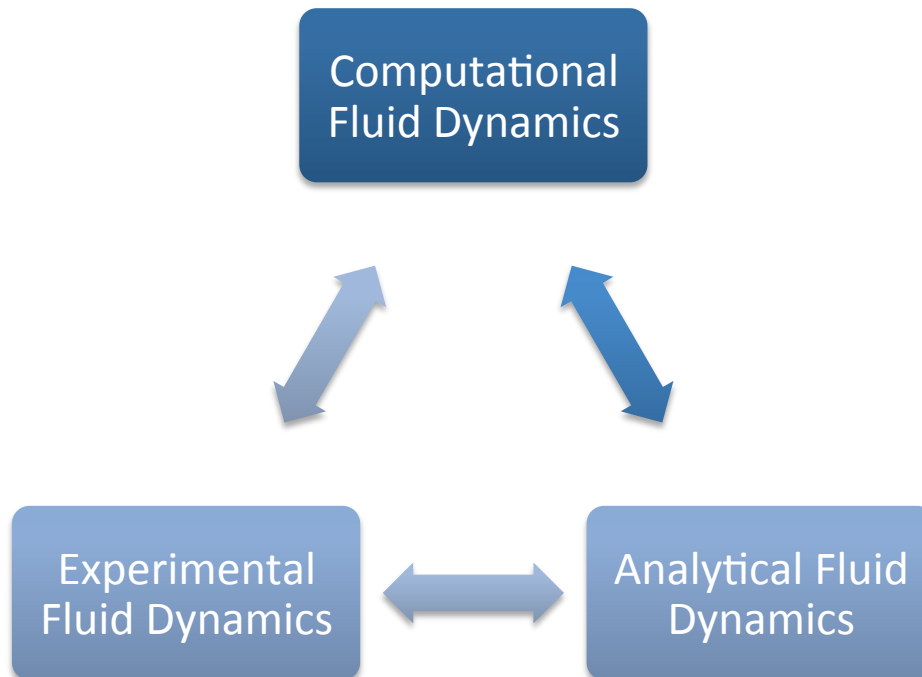


**Figure 2.2** The three basic approaches to solve problems in fluid dynamics and heat transfer. [2]

## 2.2 ADVANTAGES OF COMPUTATIONAL FLUID DYNAMICS

With the rapid advancement of digital computers, CFD is poised to remain at the forefront of cutting edge research in the sciences of fluid dynamics and heat transfer. Also, the emergence of CFD as a practical tool in modern engineering practice is steadily attracting much interest and appeal.

There are many advantages in considering CFD. The theoretical development of the computational sciences focuses on the construction and solution of the governing equations and the study of various approximations to these equations [2]. CFD complements experimental and analytical approaches by providing an alternative cost-effective means of simulating real fluid flows. Particularly, CFD substantially reduces lead times and costs in designs and production compared to experimental-based approach and offers the ability to solve a range of complicated flow problems where the analytical approach is lacking [2]. CFD has the capacity of simulating flow conditions that are not

reproducible in experimental tests found in geophysical and biological fluid dynamics, such as nuclear accident scenarios or scenarios that are too huge or too remote to be simulated experimentally (e.g., Indonesian Tsunami of 2004). Furthermore, CFD can provide rather detailed, visualized, and comprehensive information when compared to analytical and experimental fluid dynamics [3]. Although CFD is advantageous, it cannot easily replace experimental testing as a method to gather information for design purposes. Despite its many advantages, the researcher must consider the inherent limitations of applying CFD. Numerical errors occur during computations; therefore, there will be differences between the computed results and reality [18].

### **2.3 NUMERICAL METHOD**

CFD codes are structured around the numerical algorithms that can handle fluid flow problems. All the CFD commercial packages available in the market have three basic elements, which divide the complete analysis of the numerical experiment to be performed on the specific domain or geometry. The three basic elements are

- i. Pre-processor
- ii. Solver
- iii. Post-Process

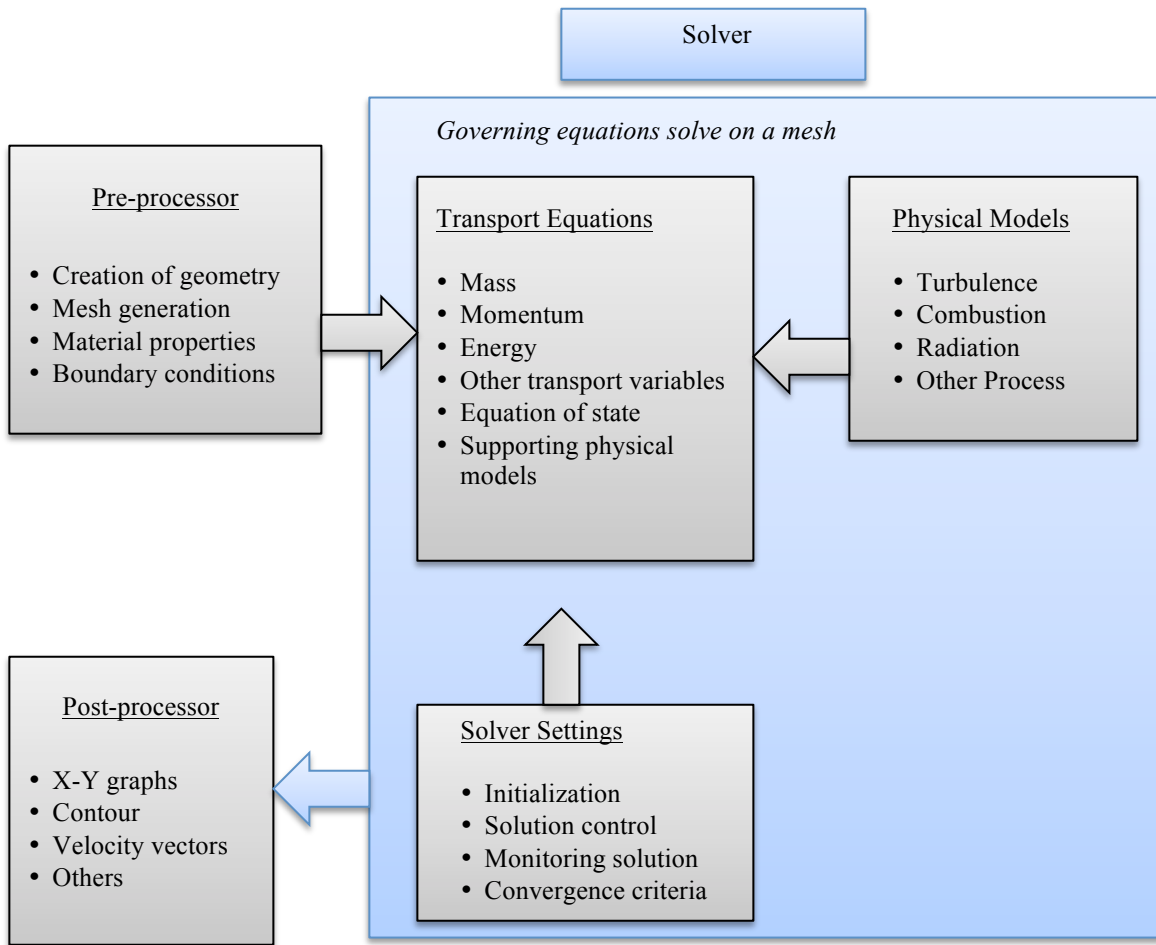


**Figure 2.3** The inter-connectivity functions of the three main elements within a CFD analysis framework. [2]

### 2.3.1 PRE-PROCESSOR

Pre-processor consists of input of a flow problem by means of a user-friendly interface and subsequent transformation of this input into form of suitable for the use by the solver. The pre-processor is the link between the user and the solver.



### **2.3.1.1 CREATION OF GEOMETRY**

This process involves several computer aided design (CAD) software like CATIA<sup>®</sup>, Solidworks<sup>®</sup>, Pro-E<sup>®</sup> and many more. The help of CAD software defines the topology of the fluid flow region of interest. This software plays a major part of the design and optimization process in research analysis.

### **2.3.1.2 MESH GENERATION**

Mesh generation constitutes one of the most important steps during the pre-process stage after the definition of the domain geometry. CFD requires the subdivision of the domain into a number of smaller, non overlapping subdomains in order to solve the flow physics within the domain geometry that has been created; this results in the generation of a mesh (or grid) of cells (elements or control volumes) overlaying the whole domain geometry. The essential fluid flows that are described in each of these cells are usually solved numerically so that the discrete values of the flow properties such as the velocity, pressure, temperature, and other transport parameters of interest are determined. This yields the CFD solution to the flow problem that is being solved. The accuracy of a CFD solution is governed by the number of cells in the mesh within the computational domain. In general, the provision of a large number of cells leads to the attainment of an accurate solution. However, the accuracy of a solution is strongly dependent on the imposed limitations dominated by the computational costs and calculation turnover times.

### **2.3.1.3 DEFINITION OF FLUID PROPERTIES**

Every surface or fluid domain has its own distinct property. The properties of the fluid used in the CFD domain are defined at this stage of the CFD Process.

#### **2.3.1.4 BOUNDARY CONDITIONS**

The complex nature of many fluid flow behaviors has important implications in which boundary conditions are prescribed for the flow problem. A CFD user needs to define appropriate conditions that mimic the real physical representation of the fluid flow into a solvable CFD problem. Every different setup of the CFD domain needs to have an initialization, which is fulfilled by the boundary conditions input [2]. The CFD code usually has this facility to define the boundary conditions of the CFD problem, where each cells at specific boundary are given finite values.

#### **2.3.2 NUMERICAL SOLVER**

The appropriate usage of either an in-house or a commercial CFD code commands the core understanding of the underlying numerical aspects inside the CFD solver. This section focuses on the treatment of the solver element. A CFD solver can usually be described and envisaged by the solution procedure presented in *Figure 2.4*

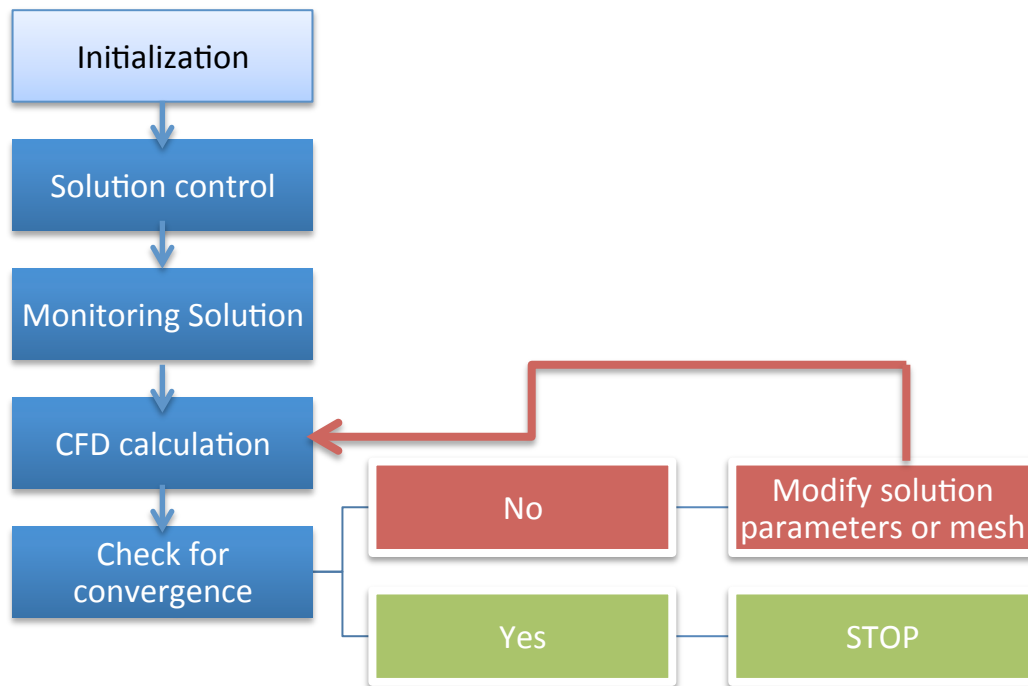


**Figure 2.4 An overview of the solution procedure [2]**

In the current market, the solvers usually use three distinct ways of calculating the solutions, namely, the finite difference method, finite element method and the finite volume method. The finite difference and finite element method are usually suitable for stress and structure analysis. On the other hand the finite volume method is the most suitable method for the CFD process. As the name implies, finite volume method is the numerical algorithm calculation process involving the use of finite volume cells. The steps involved in this solving process are usually carried out in the following sequence:

- i. Formal integration of the governing equations of fluid flow over all the control volumes or finite volumes of the solution domain.
- ii. The conversion of the integral forms of the equations into a system of algebraic equations.
- iii. Calculations of the algebraic equations by an iterative method.

### **2.3.3 POST PROCESSOR**

Commercial CFD codes such as ANSYS<sup>®</sup> Inc., CFX<sup>®</sup>, ANSYS Fluent<sup>®</sup>, STAR-CD<sup>®</sup>, and others often incorporate impressive visualization tools within their user-friendly GUIs to allow users to graphically view the results of a CFD calculation at the end of a computational simulation. Those data visualization tools of the CFD solver to observe the following results of the simulation:

- i. Domain geometry and Grid display
- ii. Vector plots
- iii. Line and shaded contour plots
- iv. 2D and 3D surface plots
- v. Particle tracking
- vi. XY plots and graphs of results

## **3 VEHICLE AND THE SPOILER**

### **3.1 INTRODUCTION TO SPOILER**

A spoiler is an automotive aerodynamic device whose intended design function is to “spoil” unfavorable air movement across a body of a vehicle in motion, usually described as drag. Spoilers on the front of a vehicle are often called air dams, because in addition to directing airflow they also reduce the amount of air flowing underneath the vehicle, which generally reduces aerodynamic lift and drag. Spoilers are often fitted to race and high-performance sports cars, although they have become common on passenger vehicles as well. Some spoilers are added to cars primarily for styling purposes and have either little aerodynamic benefit or even make the aerodynamics worse.

The goal of many spoilers used in passenger vehicles is to reduce drag and increase fuel efficiency. Passenger vehicles can be equipped with front and rear spoilers. Front spoilers, found beneath the bumper, are mainly used to decrease the amount of air

going underneath the vehicle to reduce the drag coefficient and lift. Sports cars are most commonly seen with front and rear spoilers. Even though these vehicles typically have a more rigid chassis and a stiffer suspension to aid in high-speed maneuverability, a spoiler can still be beneficial. This is because many vehicles have a fairly steep downward angle going from the rear edge of the roof down to the trunk or tail of the car, which may cause airflow separation. The flow of air becomes turbulent and a low-pressure zone is created, increasing drag and instability. Adding a rear spoiler could be considered as making the air "see" a longer, gentler slope from the roof to the spoiler, which helps to delay flow separation and the higher pressure in front of the spoiler can help reduce the lift on the car by creating down force. This may reduce drag in certain instances and will generally increase high-speed stability due to the reduced rear lift. Due to their association with racing, consumers often view spoilers as "sporty".

## **3.2 GENERIC MODELS**

### **3.2.1 VEHICLE GENERIC MODELS AND DIMENSIONS**

The Generic model of the vehicle is shown in *Figure 3.1* and *Figure 3.2* below with relevant dimensions. The length of the model is 479 cm, the width of the model is 191 cm, and the height of the model is 159 cm.

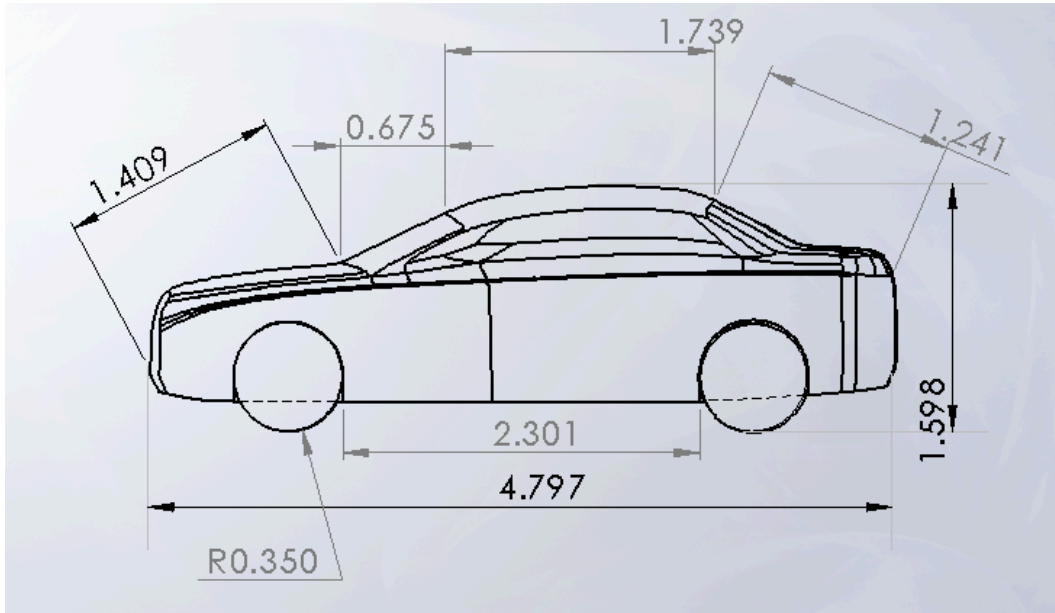


**Figure 3.1** Dimensions of the generic vehicle model [side-view]

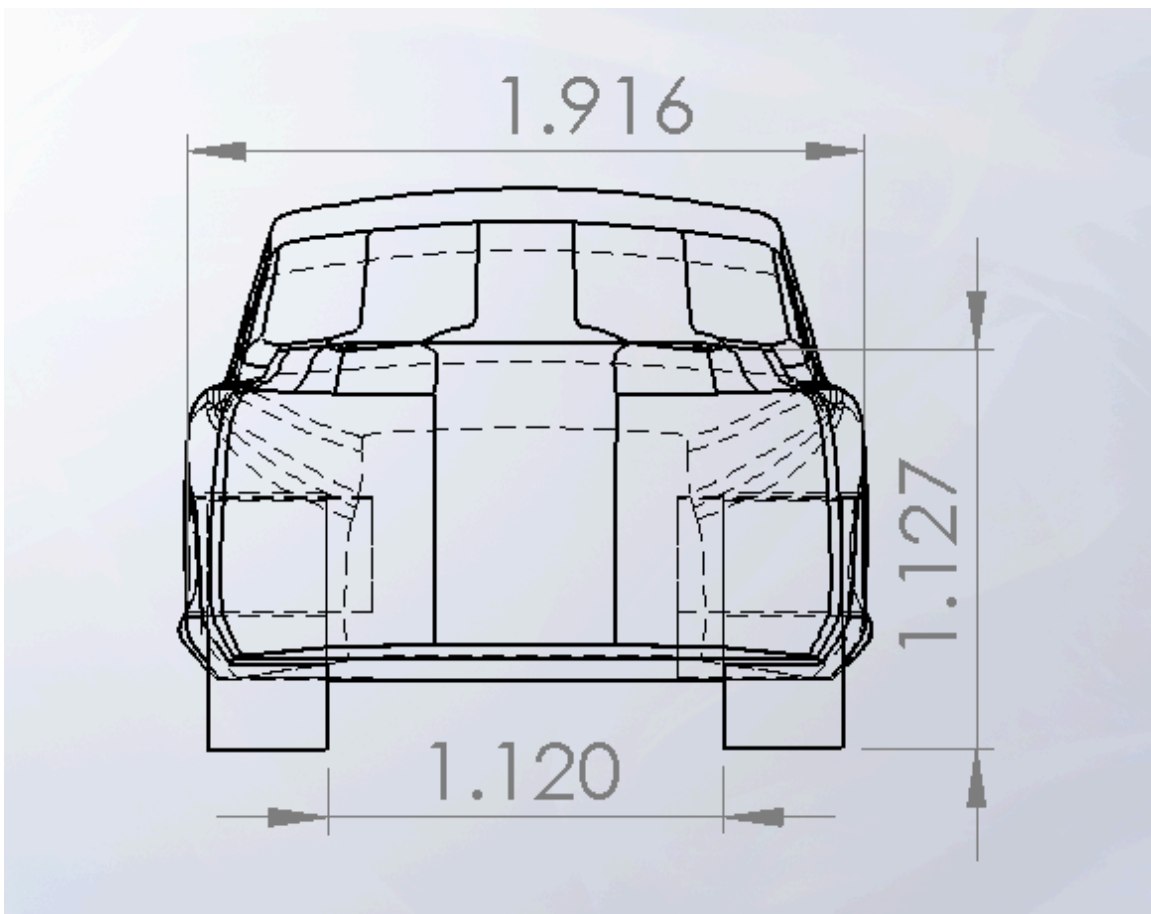


**Figure 3.2** Dimensions of the generic vehicle model [back-view]

### 3.2.2 SPOILER GENERIC MODELS AND DIMENSIONS

In the numerical analyze, two different spoiler styles have been used. The first spoiler was a “wing” style spoiler, which was mounted 23 cm above the surface of the vehicle’s rear-end, on the other hand the second spoiler was mounted edge of the rear side of the vehicle without leaving a gap between spoiler and the surface of vehicle. The generic model of the first spoilers is shown in **Figure 3.3** below, while the generic model of second spoilers is shown in **Figure 3.4**, with relevant dimensions.

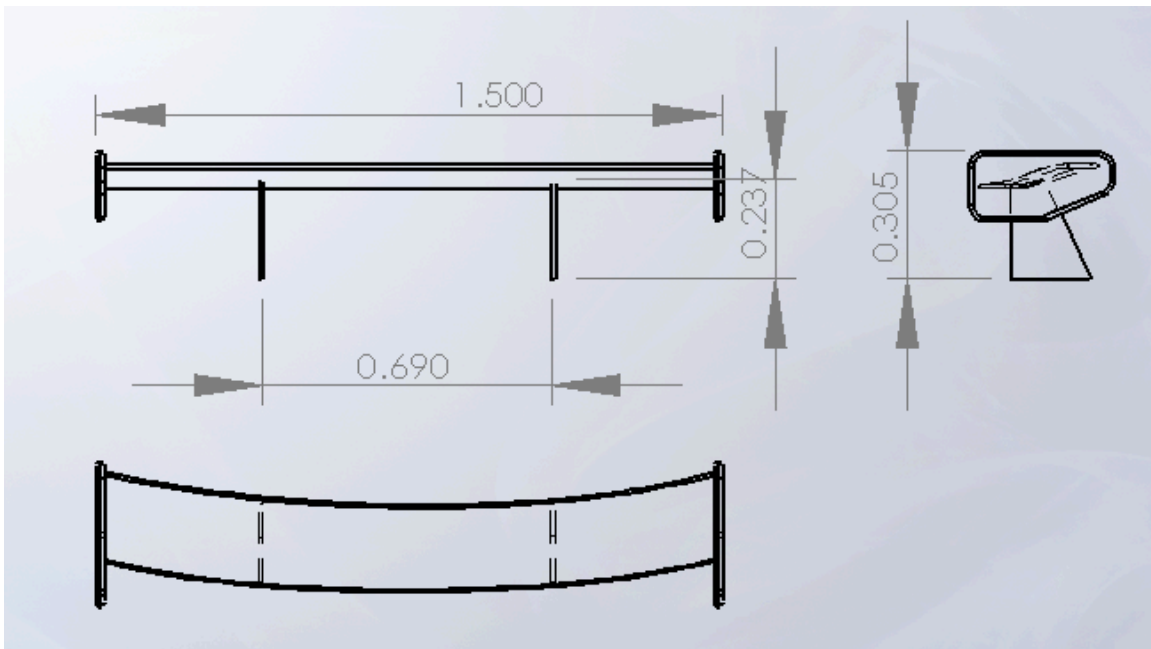


**Figure 3.3** Generic model and dimensions of first spoiler (*dimensions are in meters*)

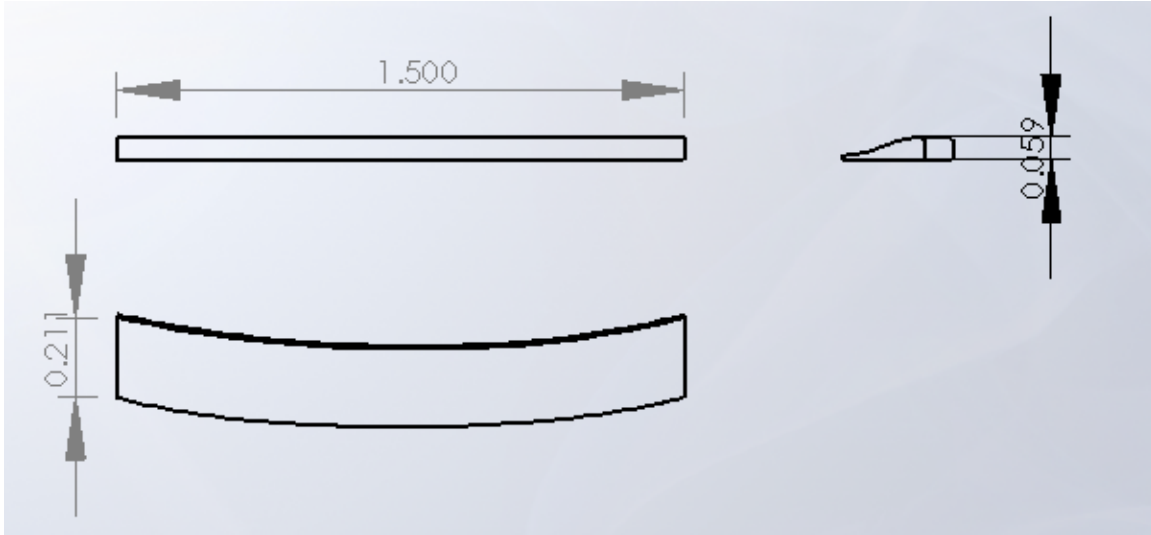


**Figure 3.4** Generic model and dimensions of second spoiler

## **4 NUMERICAL SIMULATION**

Numerical simulations have been performed on the vehicle (with/without spoiler) 3D CAD models using the CFD techniques. The software used for the numerical analysis was ANSYS FLUENT<sup>®</sup>.

### **4.1 CAD MODELS**

The models of both vehicle and two different spoilers have been 3D printed using the software called SolidWorks<sup>®</sup> to CAD format for numerical analysis.



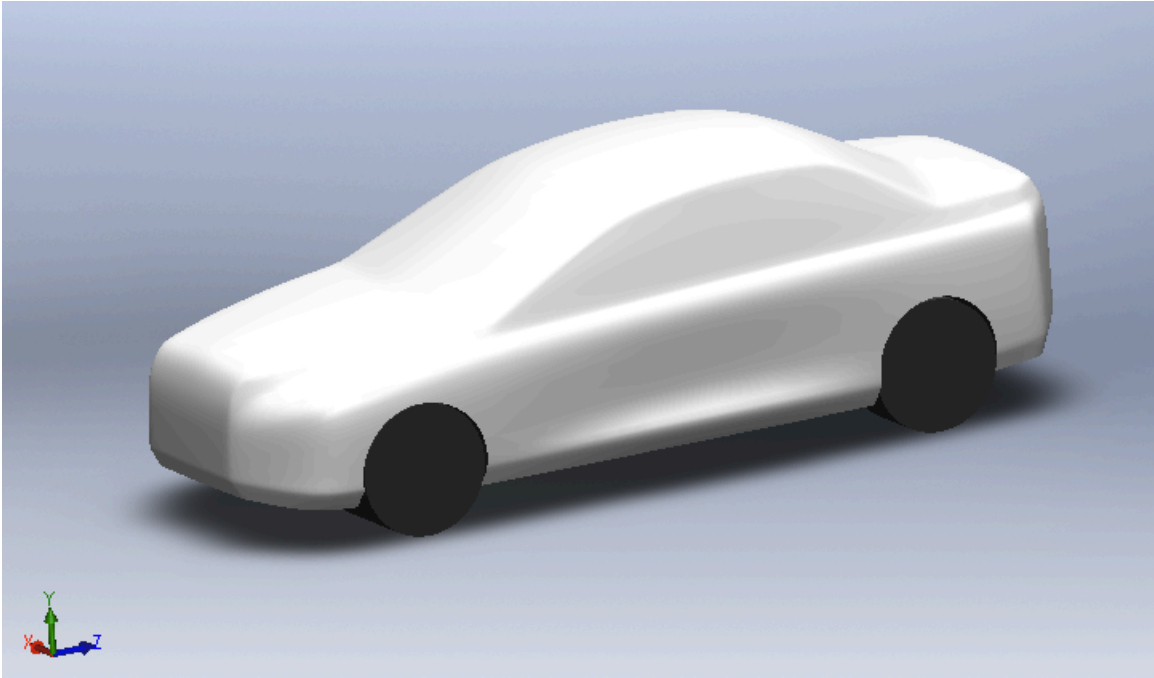


*Figure 4.1* Vehicle 3D CAD model

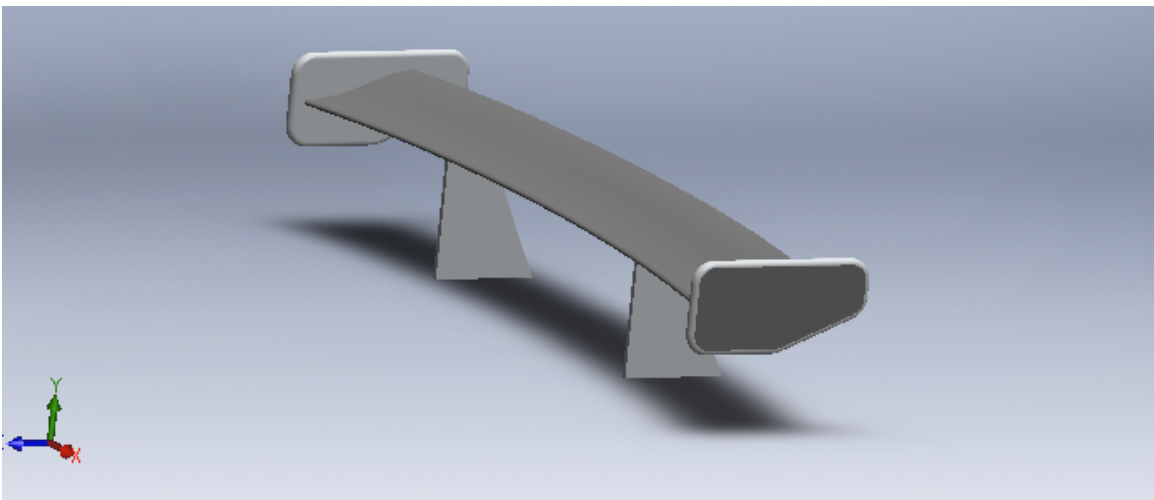


*Figure 4.2* First spoiler 3D CAD model

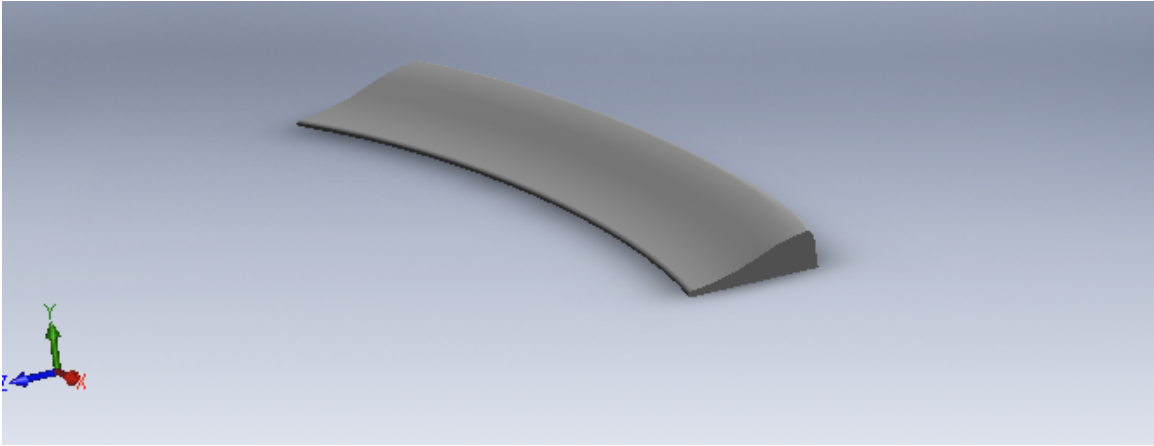


**Figure 4.3 Second spoiler 3D CAD model**

Spoilers were mounted in a rear portion of a vehicle with using “assembly” functionality of SolidWorks<sup>®</sup>. These assembled models are now ready to use for numeral analysis.

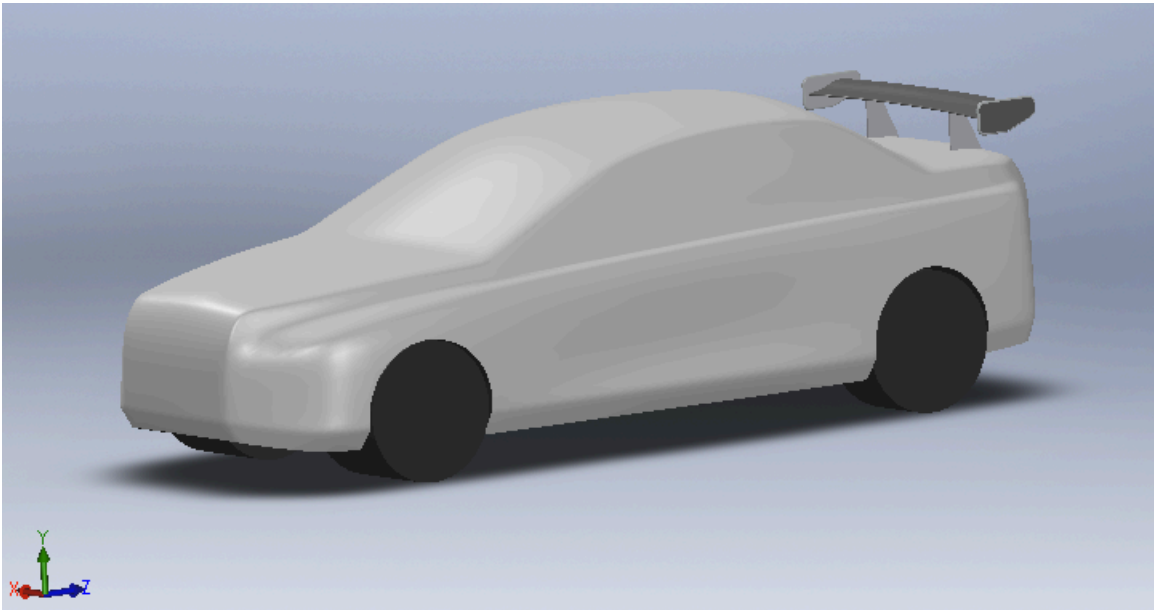


**Figure 4.4 Assembly 3D CAD model of vehicle and first spoiler**

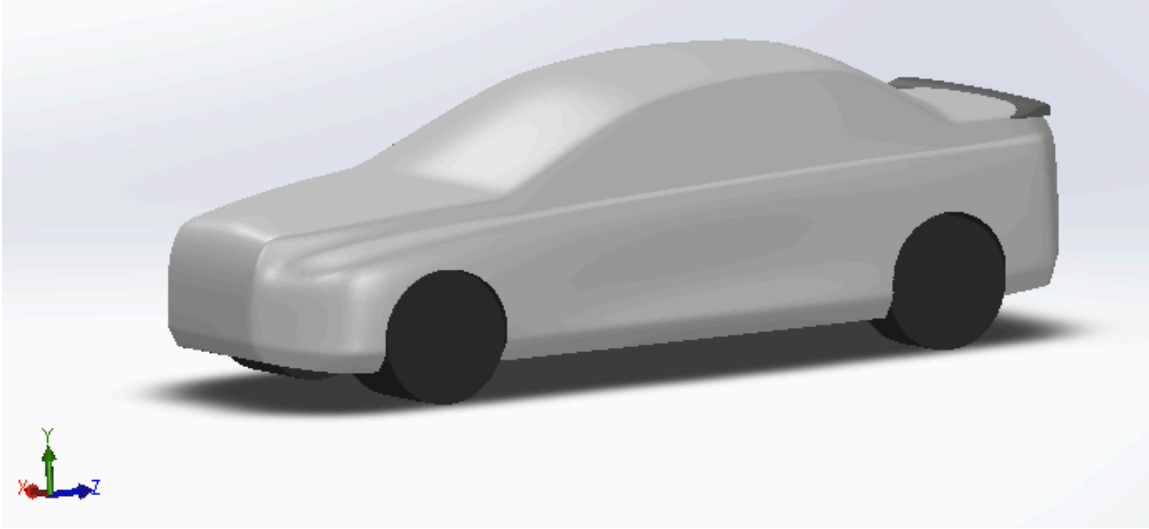


**Figure 4.5** Assembly 3D CAD model of vehicle and second spoiler

## **4.2 VIRTUAL WIND TUNNEL AND VEHICLE ORIENTATION**

The vehicle itself (*Figure 4.1*), vehicle with first spoiler (*Figure 4.4*) and vehicle with second spoiler (*Figure 4.5*) 3D CAD models shown above have been orientated in the virtual wind tunnel one-by one to performed three cases, benchmark #1, benchmark #2 and benchmark #3. A virtual air-box has been created around the 3D CAD model (*Figure 4.6*), which represents the wind tunnel in the real life. Since we are more interested in the rear side of vehicle, which is where the “wake of vehicle” phenomenon occurs, more space has been left in the rear side of the vehicle model to capture the flow behavior mostly behind the vehicle.

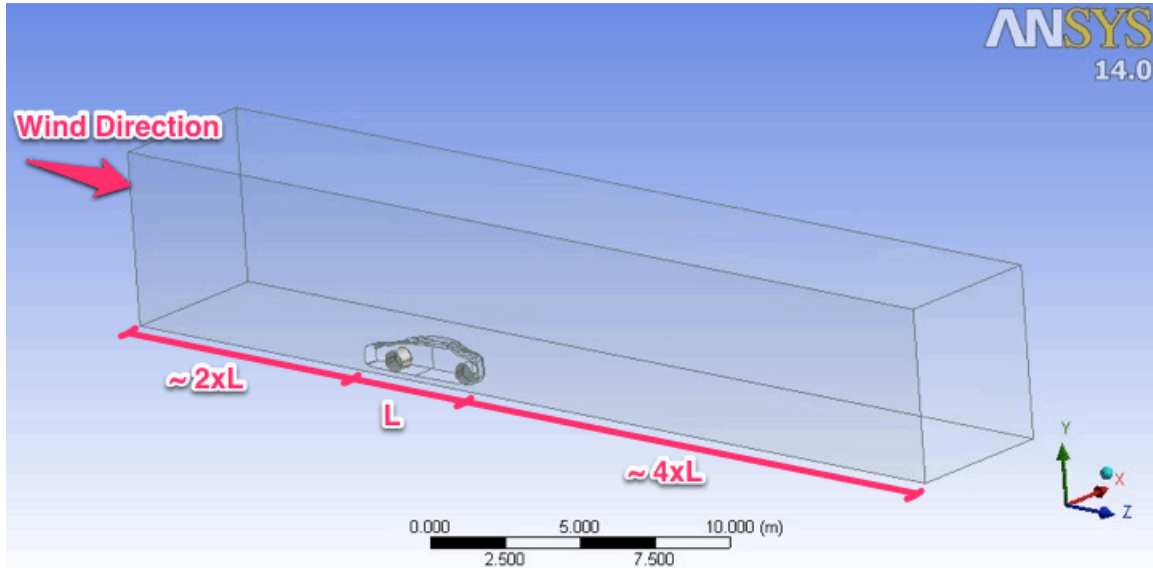
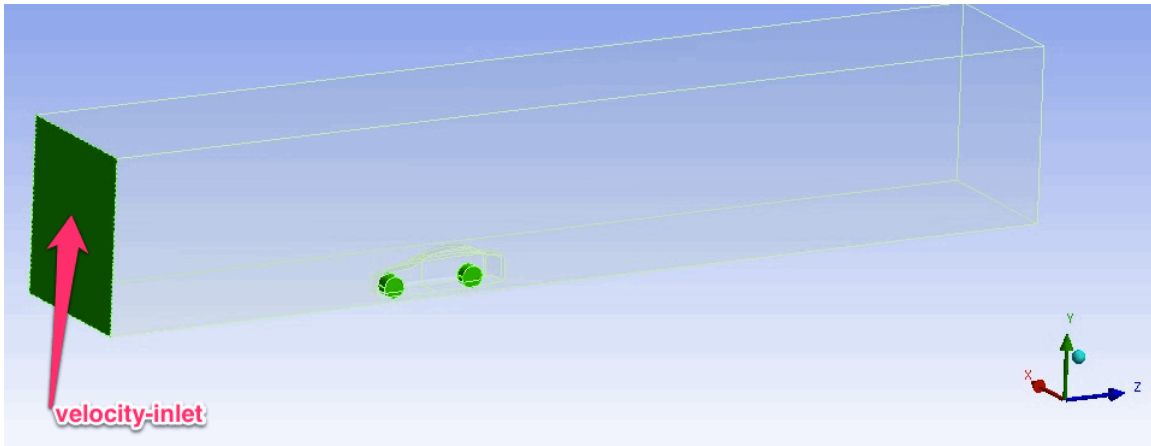
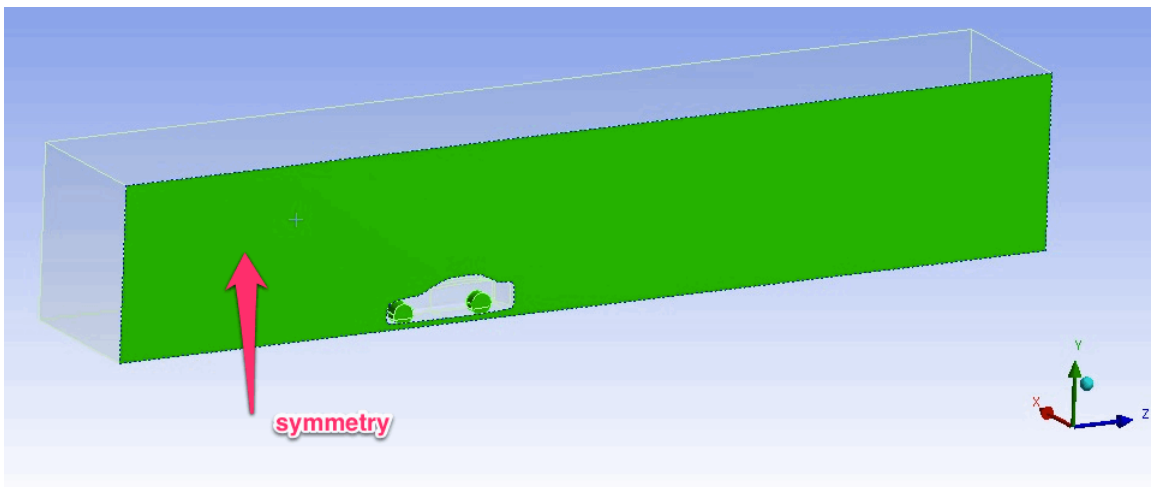


**Figure 4.6 Virtual wind tunnel and the vehicle orientation**

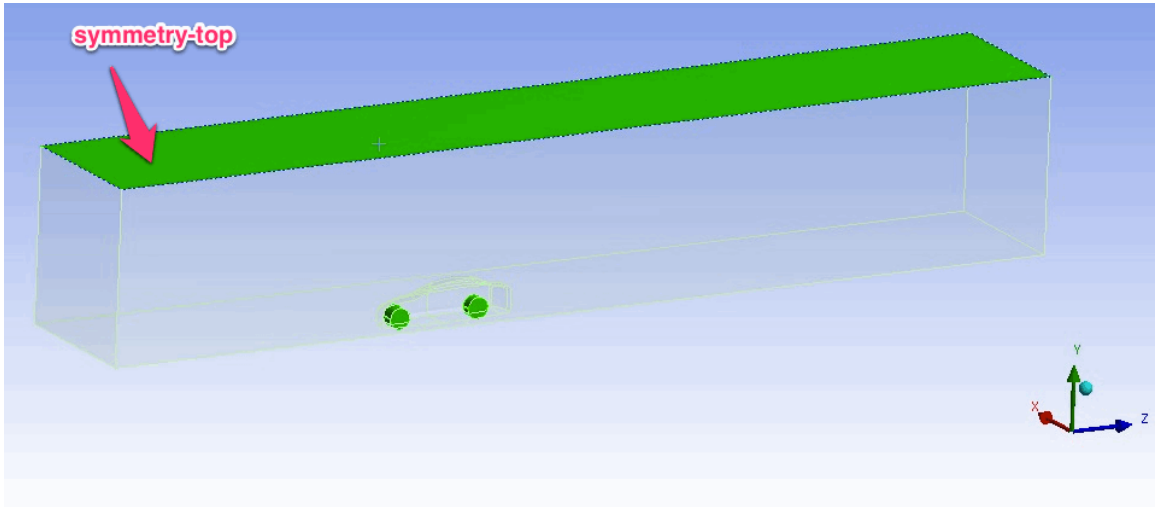
Due to the complexity of the simulation with limited computer resources and time, the complete domain was divided to half using a symmetry plane (YZ plane), which means, the simulation would be calculated for just the one side of the vehicle and since the other side is symmetric and YZ plane has been defined as symmetric boundary in the solver to make the boundary condition as “a slip wall with zero shear forces”; the simulation results would be valid for full model as well. All 6 surfaces of the virtual wind tunnel (air-box) have been named (**Figure 4.7**) so the numerical solver of ANSYS FLUENT<sup>®</sup> would recognize them and apply the appropriate boundary conditions automatically.



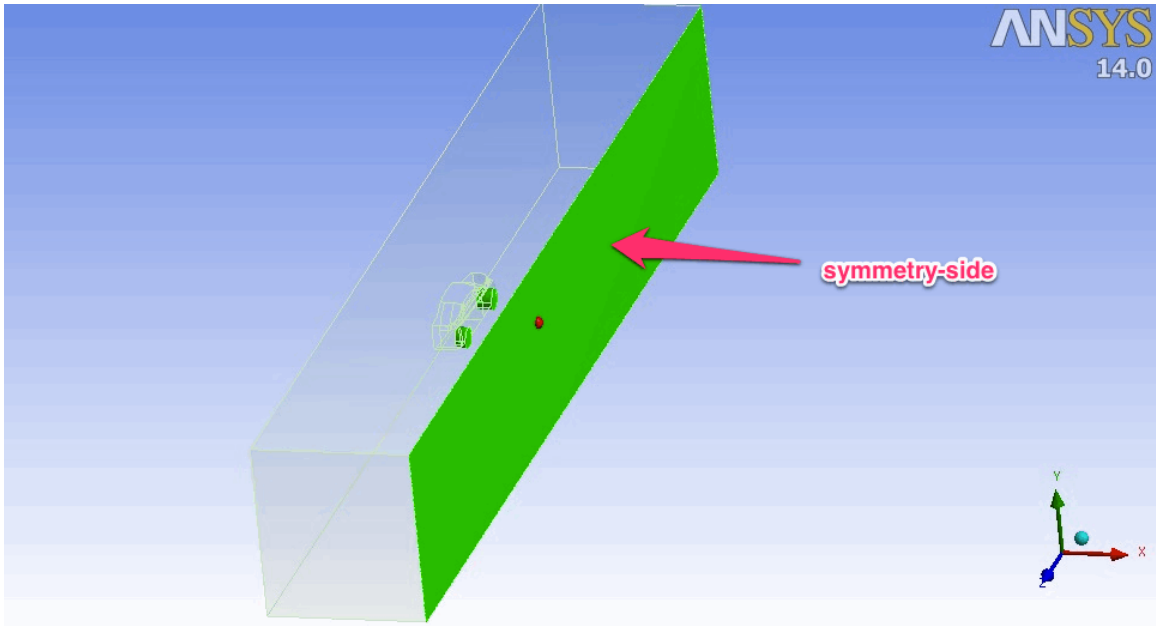
a) Velocity-inlet



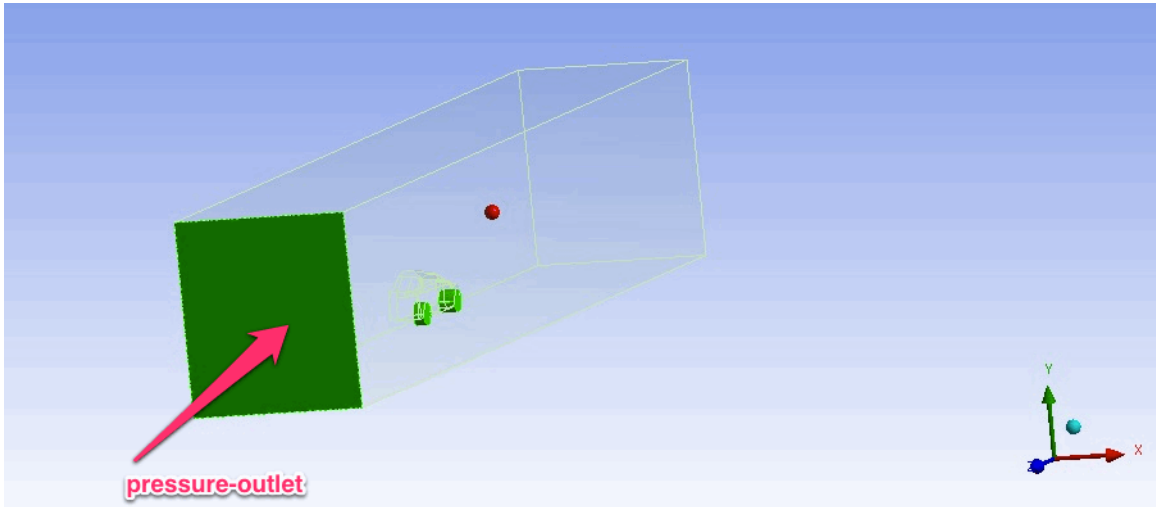
b) Symmetry



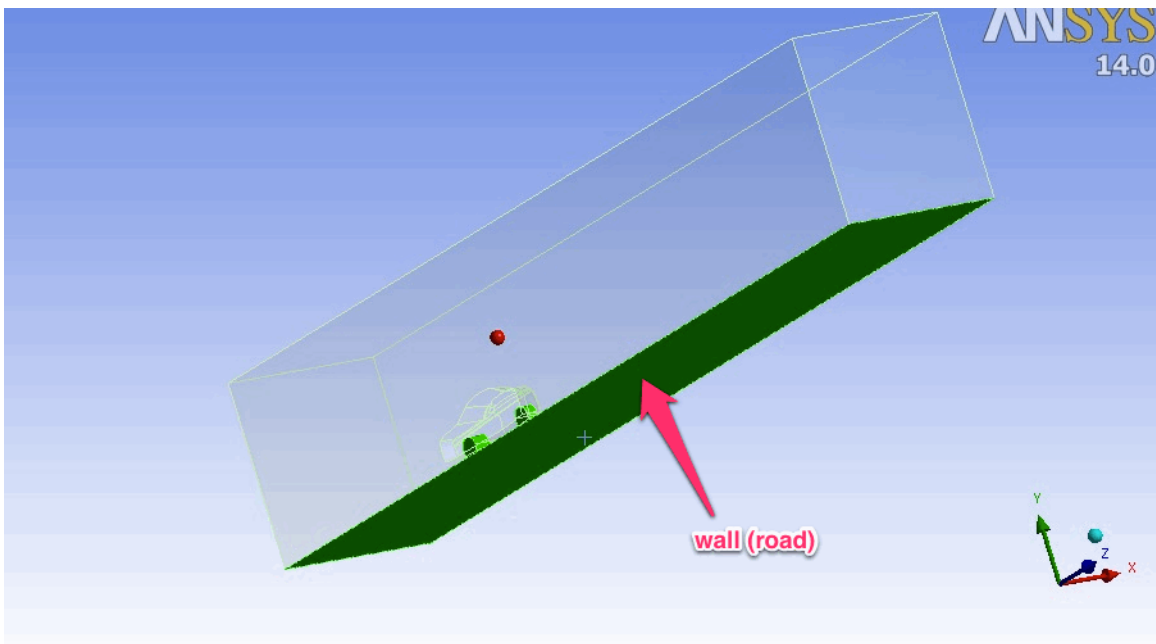
c) Symmetry-top



d) Symmetry-side



e) Pressure-outlet



f) Wall

**Figure 4.7** Virtual wind tunnel surface labeling for automatic appropriate boundary conditions. a) Velocity-inlet, b) Symmetry, c) symmetry-top, d) symmetry-side, e) pressure-outlet, f) wall

Since the right and top surfaces of the car-box was way far away from the vehicle and has no influence on the vehicle at all; they were named as “symmetry-top” and

“symmetry-side” which was for not because they were symmetric but to give them the same boundary conditions as symmetric surface (which is slip wall with zero shear forces)

### 4.3 MESH GENERAION

#### 4.3.1 MESH SIZING AND INFLATION

The triangular shape surface mesh was used due to its proximity to changing curves and bends. These elements easily adjust to the complex bodies used in automobile and aerospace bodies. With the default settings for mesh generation, ANSYS Meshing<sup>®</sup> has generated the meshes as seen in *Figure 4.8*. This coarse meshing with the standard settings was used to run benchmark #1 which will be discussed in the next chapter.

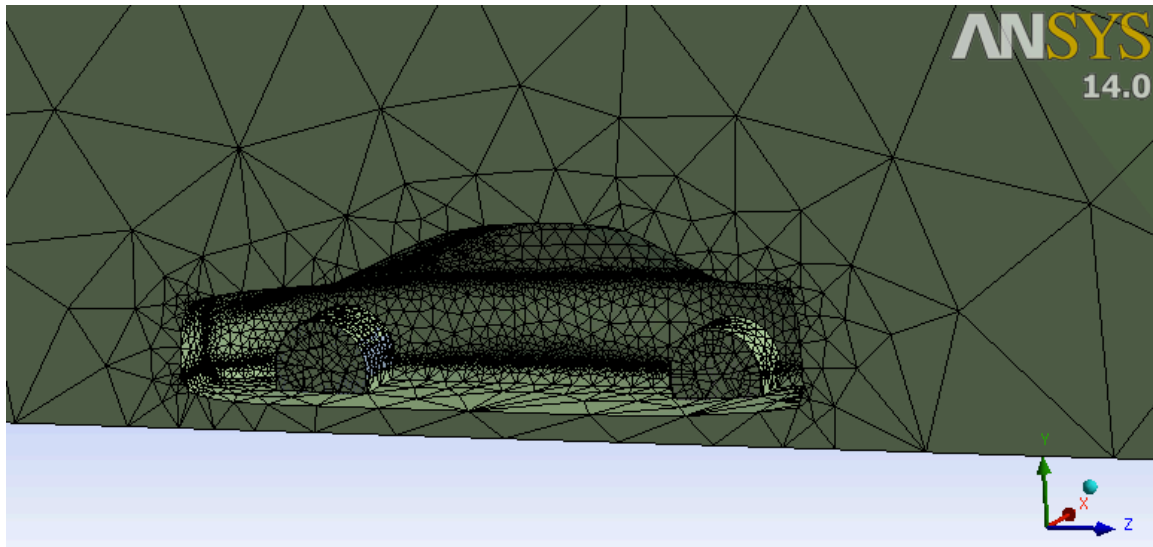


**Figure 4.8** Mesh generation with standard settings.

With the global mesh sizing settings, ANSYS Meshing<sup>®</sup> recognized that there were some curvatures around the vehicle body. But the meshing was very coarse and it was only the initial guess by the software. In order to capture more accurate data through solver we needed to improve the mesh. The first thing to do was changing the mesh sizing parameters. All meshing sizing parameters that have been altered are given in the



**Table 4-a.** As seen in **Figure 4.9** ANSYS Meshing<sup>®</sup> has generated the meshes with the new sizing parameters that are given in the **Table 4-a**.

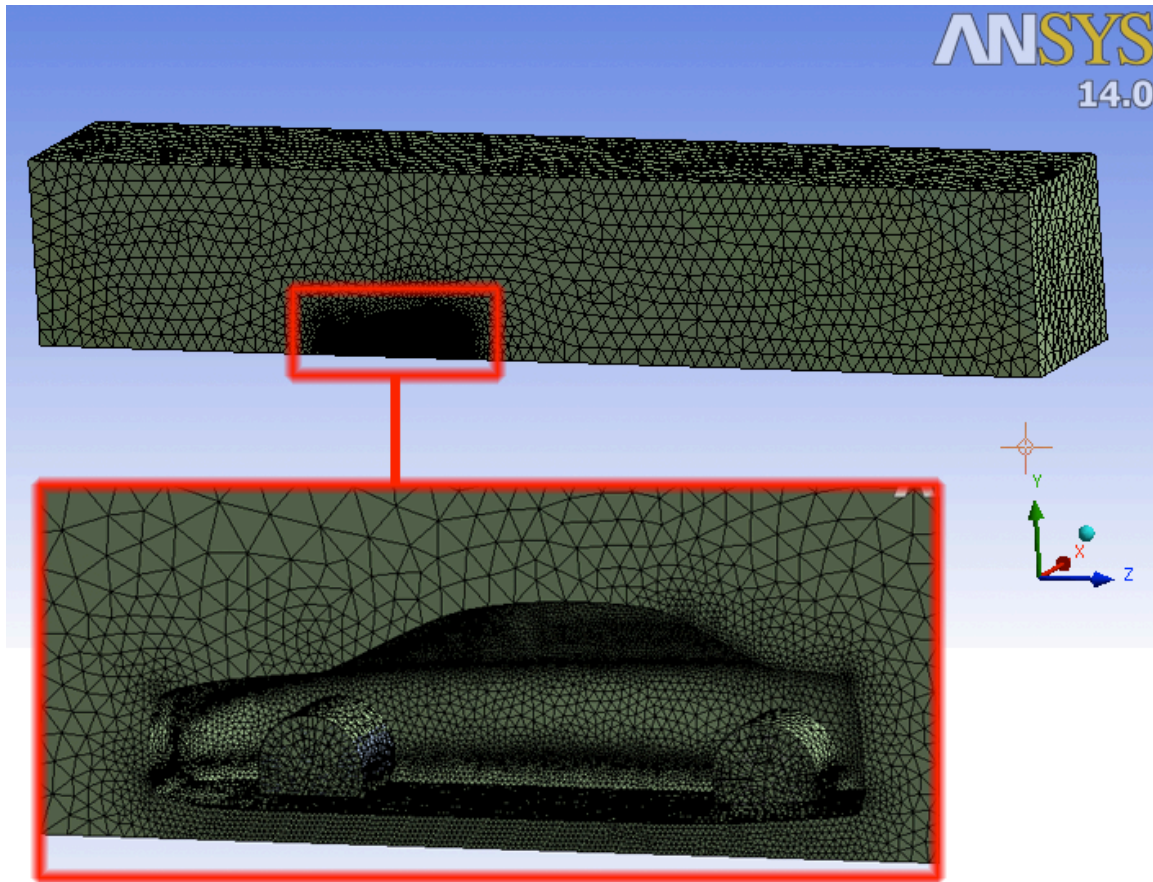


**Figure 4.9** Mesh generation with modified sizing settings.

The new mesh looked more decent but still it was lack of inflation layer around the vehicle body. The inflation layer has been enabled and “Automatic inflation: Program Controlled” has been set to capture the boundary effects of the flow around the body more accurately. The vehicle body itself and the road have been included to “program controlled inflation” while the other named selections (velocity-inlet, pressure-outlet, symmetry etc.) are excluded. Based on what is advised for vehicle external aerodynamics with ANSYS FLUENT<sup>®</sup> by Marco Lanfrit [7] guideline, the inflation option has been set as “First Aspect Ratio” instead of “Smooth Transition” (which was the default value).

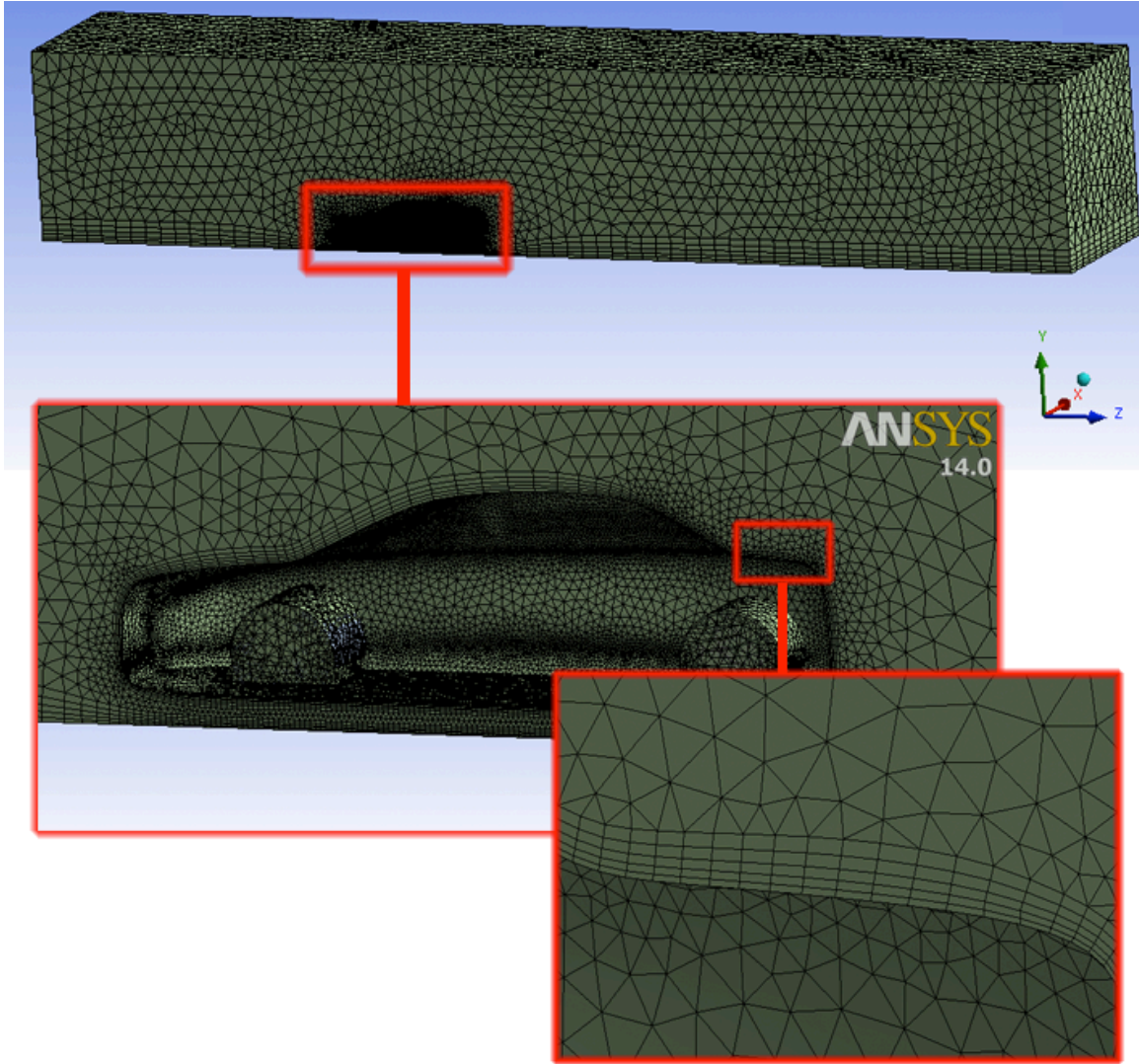


**Figure 4.10** Mesh generation with the inflation layers

*Figure 4.10* shows the new mesh after the automatic inflation has been enabled as “program controlled” and the inflation option has been selected as “first aspect ratio”. Another recommendation from the guideline by Fluent Germany [7] is to create a new volume control box around the body where the elements can be limited to a certain size; just like how the standard meshing sizes were limited to minimum 17.823 mm and maximum 500 mm through the entire domain. The advantage of using a control volume and limiting the mesh sizing within the control volume only, lets us to improve the meshing quality only within in the area where we need high resolution mesh; instead of having fine mesh in the entire domain which would eliminate the time consumption to

run the simulation and leads us to get decent results quickly. There are several ways doing this, one of them is to create a “sphere of influence”, but this method is used usually for helicopter or airplane simulation mostly when there is no wall (or road) involved. Another way of doing this is to create a virtual box around the vehicle that is 2.5 times longer in the z-direction, and 1.5 times longer in the x and y-directions. The orientation of this virtual box (which was called as “car-box”) can be seen in **Figure 4.11**.

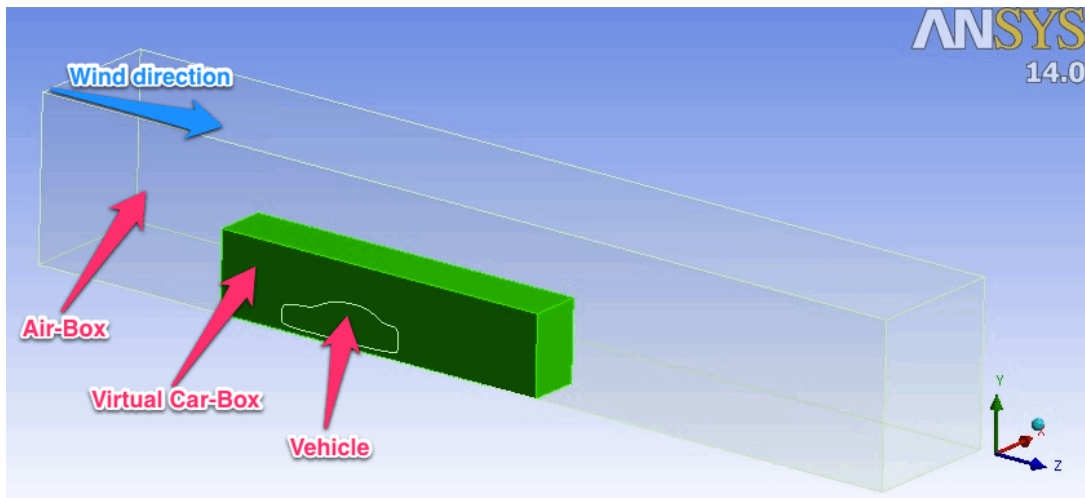


**Figure 4.11 Virtual car-box orientation**

The virtual car-box was orientated as seen in **Figure 4.11** and it can be noticeable in the figure that there is more space at the backside than the front side of the vehicle. It is because we are more interested in behavior of the airflow at the backside of vehicle after it passes the vehicle. Once the virtual car-box was generated and its mesh sizing was limited to 80mm with the “body sizing” functionality in the software, the new mesh became very detailed and ready to run in the solver. The final meshing can be seen in **Figure 4.12**. The same procedure to create high resolution meshing has been followed for all cases (Case #1: Vehicle itself, Case #2: Vehicle with first spoiler, Case #3: Vehicle with second spoiler) exactly the same.



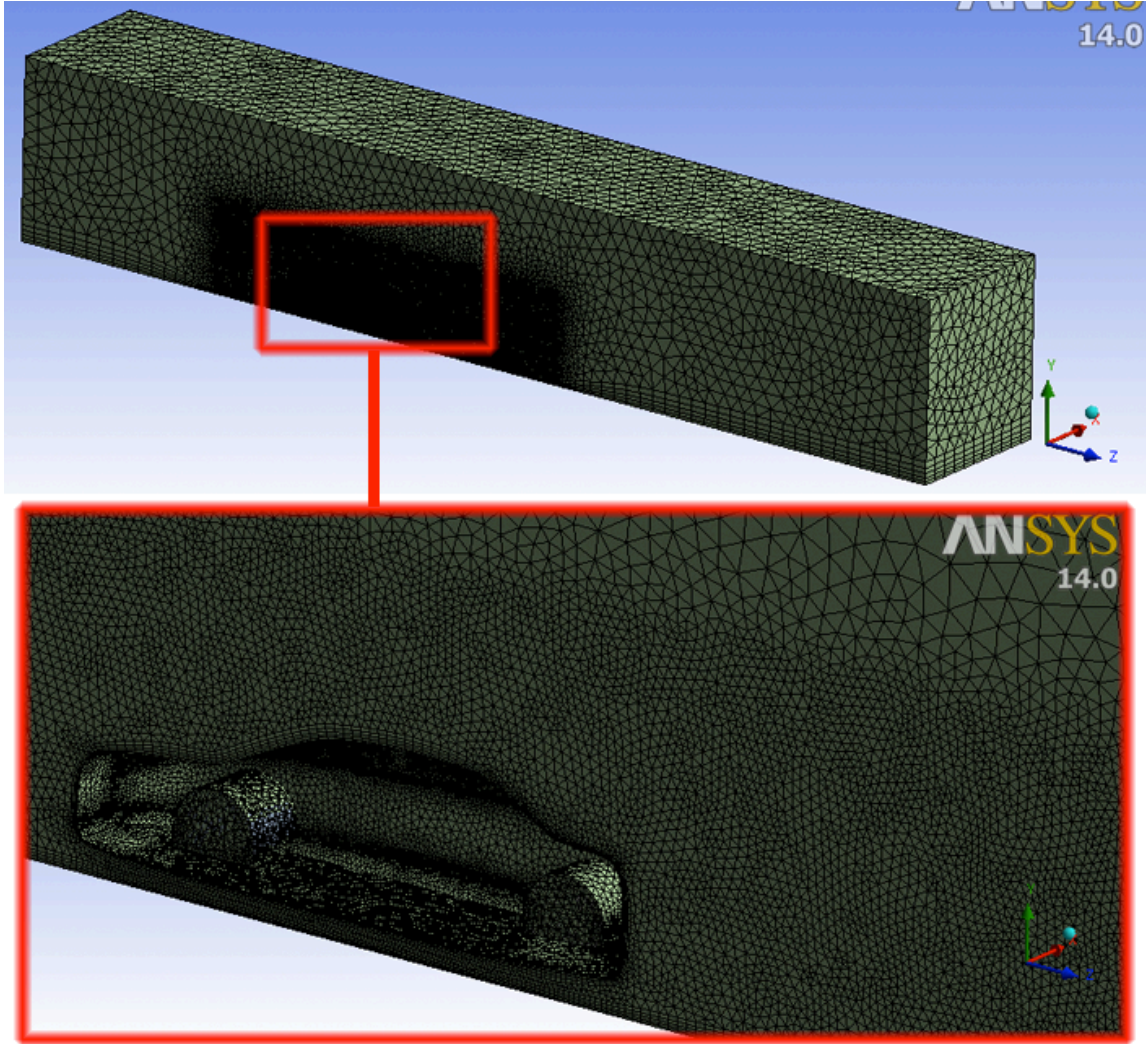


*Figure 4.12* The final mesh

	<b>Case #1, Case #2, Case #3, Benchmark #3</b>	<b>Benchmark #1</b>	<b>Benchmark #2</b>
<b><i>Global Mesh Sizing Settings</i></b>			
Use Adv. Size Fun.	On: Proximity and Curvature	On: Curvature	
Relevance Center	Coarse	Coarse	
Initial Size Speed	Active Assembly	Active Assembly	
Smoothing	High	Medium	
Transition	Slow	Slow	
Span Angle Center	Fine	Fine	
Curvature Nor. Angle	12.0°	18.0°	12.0°
Proximity Accuracy	0.5	-	
Minimum Size	17.823mm	17.823mm	
Maximum Size	500mm	3,564mm	
Growth Rate	1.20 (20%)		
<b><i>Inflation</i></b>			
Use Automatic Inflation	Program Controlled	-	Program Controlled
Inflation Option	First Aspect Ratio	-	First Aspect Ratio
First Aspect Ratio	5	-	5
Maximum Layers	5	-	5
Growth Rate	1.2 (20%)		
<b><i>Virtual Car-Box (body sizing)</i></b>			
Type	Body of Influence	-	-
Element Size	80mm	-	-
<b><i>Figures</i></b>	<b><i>Figure 4.12</i></b>	<b><i>Figure 5.12</i></b>	<b><i>Figure 5.16</i></b>

**Table 4-a Mesh sizing parameters**

#### 4.4 VALIDATION PROCEDURE

Good engineering practice suggests that prior to using an analysis technique on a new configuration, one should benchmark the technique against a known (respected) initial case or test case similar to the new configuration. The validation assessments of a CFD simulation that have been used in this thesis can be summarized as

❖ Examine iterative convergence

Validation assessment requires that a simulation demonstrate iterative convergence.

❖ Examine grid convergence

The examination of the spatial convergence of a simulation is a straightforward method for determining the ordered discretization error in a CFD simulation. The method involves performing the simulation on two or more successively finer grids. The term grid convergence study is equivalent to the commonly used term grid refinement study. I wanted to determine the error band for the engineering quantities obtained from the finest grid solution. However, if the CFD simulations are part of a design study that may require tens or hundreds of simulations, which is the case of this thesis, then one of the coarser grids should be used. Thus I also wanted to be able to determine the error on the coarser grid. The benchmark #1 has been performed to compare the results between fine resolution grids and coarse resolution grids while the benchmark #2 has been performed to find out how the resolution is effective in terms of getting decent results and to find out how the solutions vary depends on the grid resolution.

❖ Compare CFD results to experimental data

Experimental data is the observation of the “real world” in some controlled manner. By comparing the CFD results to experimental data, one hopes that there is a good agreement, which increases confidence that the physical models and the code represents the "real world" for this class of simulations. However, no (trusted) experimental data has

been found to compare the CFD simulation results, so this validation assessment doesn't work for this thesis at all.

❖ Examine model uncertainties

The physical models in the CFD code contain uncertainties due to a lack of complete understanding or knowledge of the physical processes. One of the models with the most uncertainty is the turbulence model. The uncertainty can be examined by running a number of simulations with the various turbulence models and examine the affect on the results. The benchmark #3 has been performed for comparing the results of using different turbulence models.

#### **4.5 SOLVER SETTINGS**

The problem of vehicle external flow numerical analysis required the solver settings to be completed before starting the simulations. The solver setting includes type of solver (3D or 2D), the viscous model, boundary conditions and solution controls. The inlet of the wind tunnel was indicated by the term “velocity-inlet”, while the outlet of the wind tunnel was termed as “pressure-outlet”. The solver settings and boundary condition for all the cases and benchmarks are shown in the tables below (*Table 4-b, Table 4-c and Table 4-d*).

	Case #1	Case #2	Case #3	Benchmark #1	Benchmark #2	Benchmark #3
Simulation	3d, pbns, rke					3d, pbns, sstkw
<b><i>Pressure-Velocity Coupling</i></b>						
Scheme	Coupled					
<b><i>Solver</i></b>						
Gradient	Least Squares Cell Based					
Iteration	<i>First Order Upwind</i> for the first 100 iterations; <i>Second Order Upwind</i> until converged					
Flow Courant Number	50					
<b><i>Explicit Relaxation Factors</i></b>						
Pressure	0.25					
Momentum	0.25					
<b><i>Under-Relaxation Factors</i></b>						
Tur. Kin. En.	0.8					
Tur. Dis. Rate	0.8					
Tur. Viscosity	0.8 for the first 100 iterations, then 0.95 until converged					

**Table 4-b Solver settings**



	Case #1	Case #2	Case #3	Benchmark #1	Benchmark #2	Benchmark #3
<b>Viscous Model</b>						
Tur. Model	$k - \varepsilon$ (2 eqn)			$k - \omega$ (2 eqn)		
$k - \varepsilon$ Model	Realizable					-
$k - \omega$ Model						Shear Stress Transport (SST)
Near-wall Treatment	Non-Equilibrium Wall Functions					-

**Table 4-c Viscous model and turbulence model settings**

<b>Boundary Conditions (for all cases and benchmarks)</b>		
<b>Velocity Inlet</b>	<i>Magnitude and Direction</i>	30m/s (Positive Z-direction)
	<i>Turbulence Specification Method</i>	Intensity and Viscosity Ratio
	<i>Turbulence Intensity</i>	1.00%
	<i>Turbulent Viscosity Ratio</i>	10
<b>Pressure Outlet</b>	<i>Gauge Pressure magnitude</i>	0 Pascal
	<i>Gauge Pressure direction</i>	Normal to boundary
	<i>Turbulence Specification Method</i>	Intensity and Viscosity Ratio
	<i>Backflow Turbulence Intensity</i>	10%
	<i>Backflow Turbulent Viscosity Ratio</i>	10
<b>Wall Zones</b>	<i>No Slip</i>	
<b>Symmetry</b>	<i>No Slip</i>	
<b>Fluid Properties</b>	<i>Fluid Type</i>	Air
	<i>Density</i>	$\rho = 1.175 \text{ kg/m}^3$
	<i>Kinematic viscosity</i>	$\nu = 1.8247 \times 10^{-5} \text{ kg/m} \cdot \text{s}$

**Table 4-d Boundary condition settings**

## 5 SIMULATION RESULTS

### 5.1 SIMULATION RESULTS OF CASE #1, CASE #2 AND CASE #3

A 3D steady state, incompressible solution of the Navier-Stokes equations was performed using ANSYS FLUENT<sup>®</sup>. Turbulence modeling was done with the realizable k- $\epsilon$  model using non-equilibrium wall functions. The computational results for the following cases are presented and discussed:

- ❖ Case #1: Vehicle model without rear-spoiler
- ❖ Case #2: Vehicle model with the first rear-spoiler design
- ❖ Case #3: Vehicle model with the second rear-spoiler design

All the results for different cases were obtained with the same meshing resolution, the same k –  $\epsilon$  turbulence model, and also the same boundary conditions. The free stream velocity was set to be 30m/s (~65mph, which is the speed limit in highways). For the first 100 iterations, a first order upwind discretization was used to accelerate the convergence then after 100 iterations second order upwind scheme has been applied and iterations have continued until it reached to the convergence criteria. The convergence criteria were having all residuals below 1e-3. The plots of residuals for all 3 different cases are given in *Figure 5.1*, *Figure 5.2* and *Figure 5.3* respectively.

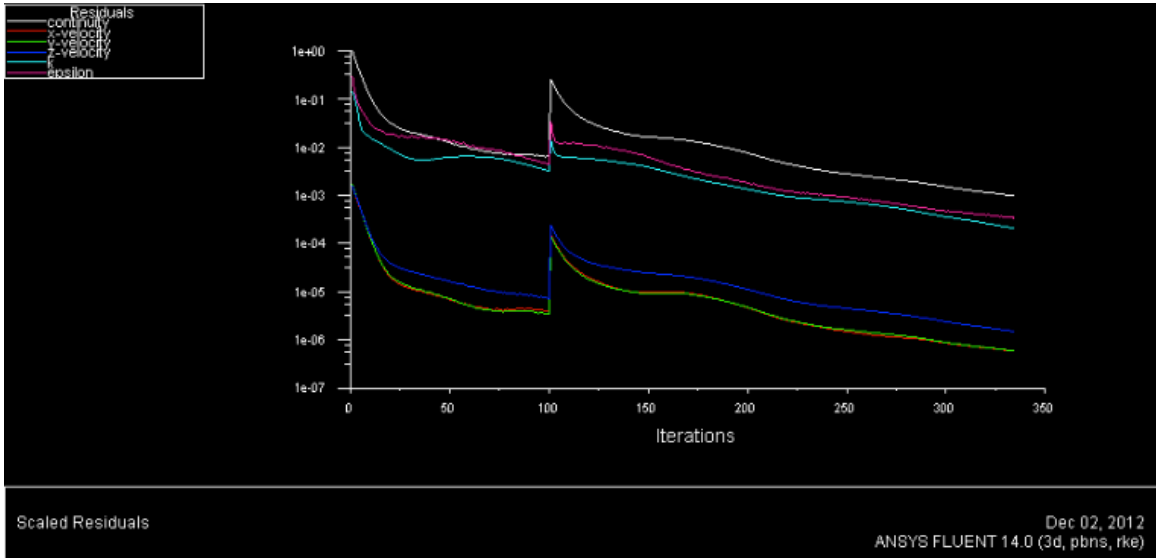


**Figure 5.1** The scaled residuals convergence history for case #1

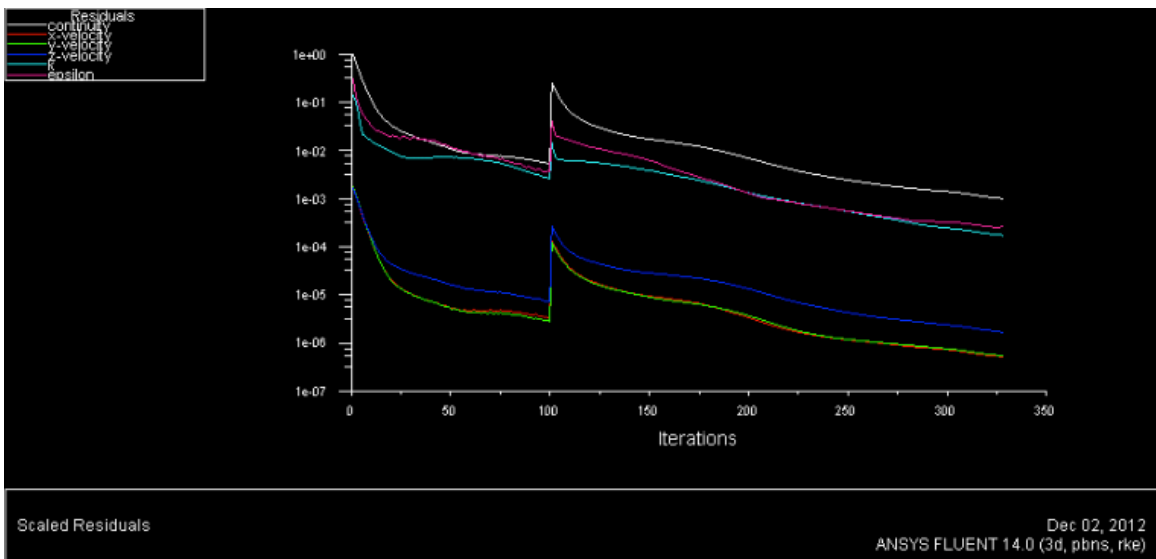


**Figure 5.2** The scaled residuals convergence history for case #2

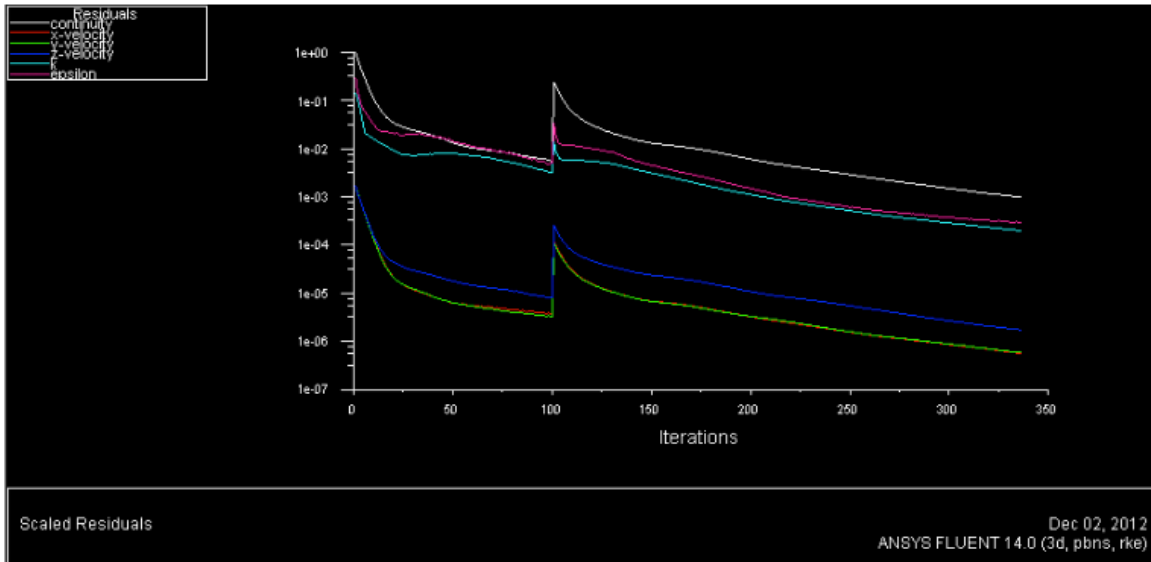


**Figure 5.3** The scaled residuals convergence history for case #3

As seen in the *Figure 5.1*, *Figure 5.2* and *Figure 5.3* residuals are jumped off at the 101<sup>st</sup> iteration because the scheme has been changed from first order upwind to second order upwind in order to reach convergence much faster.

*Figure 5.4* shows the convergence history of drag coefficient of case #1 and case #2. In both cases, the drag coefficient has converged very quickly and changed only by 1-2% after the 200<sup>th</sup> iteration (which is 100 iterations more after the second order upwind scheme was applied).

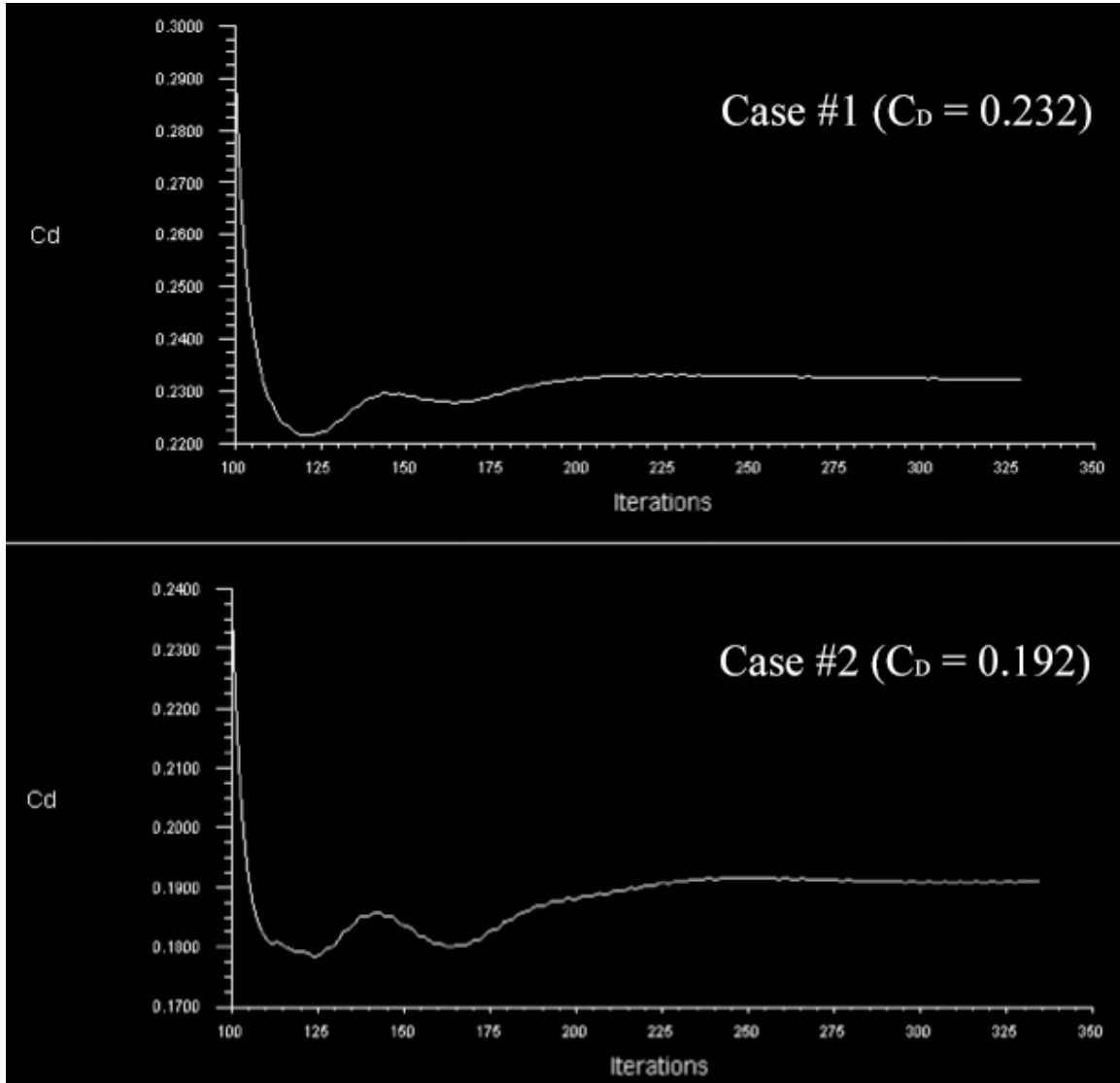


**Figure 5.4 Drag coefficient ( $C_D$ ) convergence histories of case #1 and case #2**

There was significant change in terms of drag force, and same thing happened in down-force (negative lift-force) over the vehicle body by having a spoiler at rear-end although the case #3 didn't give the as big effect as case #2 - drag coefficient has dropped down to 0.217 only. Since Case #2 and Case #3 have exactly same meshing resolution, the same  $k - \epsilon$  turbulence model, and also the same boundary conditions, it has been found that the drag reduction by having spoiler at the rear end of the vehicle is very much dependent on the shape (design) of the spoiler. On the other hand, case #3 generated significant down-force (negative lift-force); the lift coefficient with the help of the second spoiler (case #3) has reduced to -0.268 while it was reduced to -0.239 with the help of the

first spoiler (case #2). The vehicle itself without any spoiler had -0.222 lift coefficient, which was our reference point. Drag and lift coefficients for all three cases are presented in **Table 5-a**.

Model	C <sub>D</sub>	C <sub>L</sub>
<b>Case #1</b> <i>(Vehicle only)</i>	0.232	-0.222
<b>Case #2</b> <i>(Vehicle + First spoiler)</i>	0.192	-0.239
<b>Case #3</b> <i>(Vehicle + Second spoiler)</i>	0.217	-0.268

**Table 5-a Drag and list coefficients for 3 cases**

The results for case #2 and case #3 (which were the cases when the two different spoilers attached at the rear end of vehicle) were compared with the results with case #1(vehicle without spoiler).

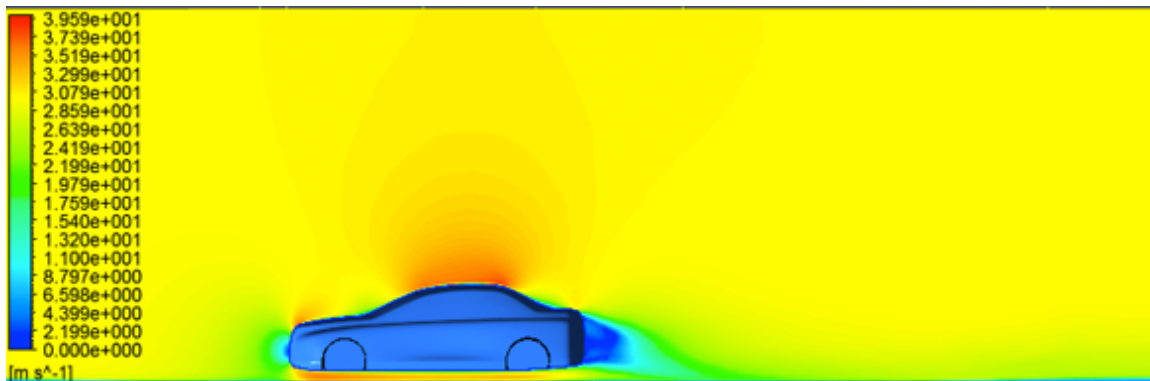


**Figure 5.5 Velocity distribution of flow in the symmetry plane for case #1 (maximum velocity: 39.59 m/s)**

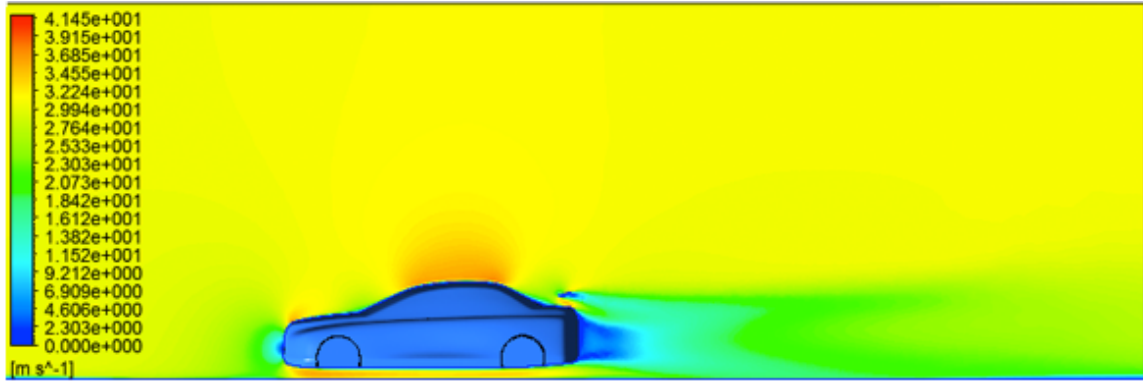


**Figure 5.6** Velocity distribution of flow in the symmetry plane for case #2 (*maximum velocity: 41.45 m/s*)

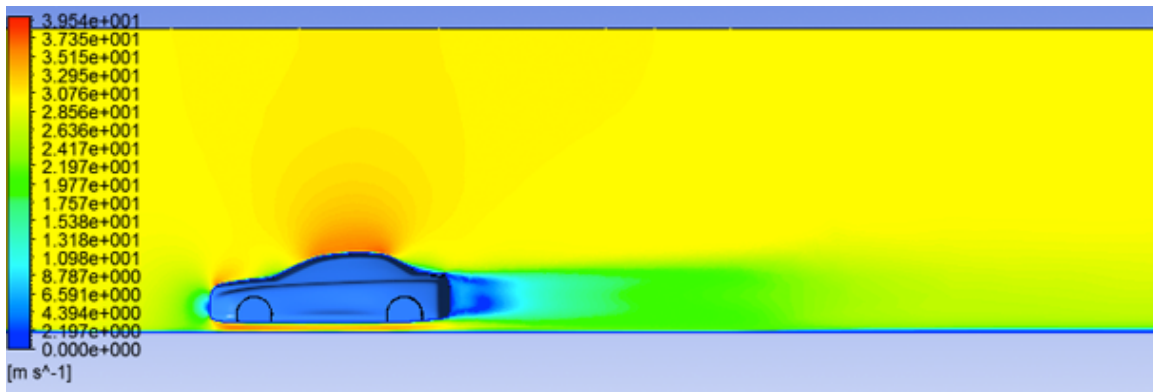


**Figure 5.7** Velocity distribution of flow in the symmetry plane for case #3 (*maximum velocity: 39.54 m/s*)

Contours of velocity for a high-speed vehicle at the symmetry plane for all 3 cases are shown in **Figure 5.5**, **Figure 5.6** and **Figure 5.7** respectively. The vehicles with rear spoiler (case #2 and case #3) had large and double air swirls at the rear end. It has been found that there were recirculation zones behind the rear end of the vehicle. By comparing the cases in figures, the recirculation zone behind the rear end of vehicle with spoiler situations (case #2 and case #3) were clearly larger.

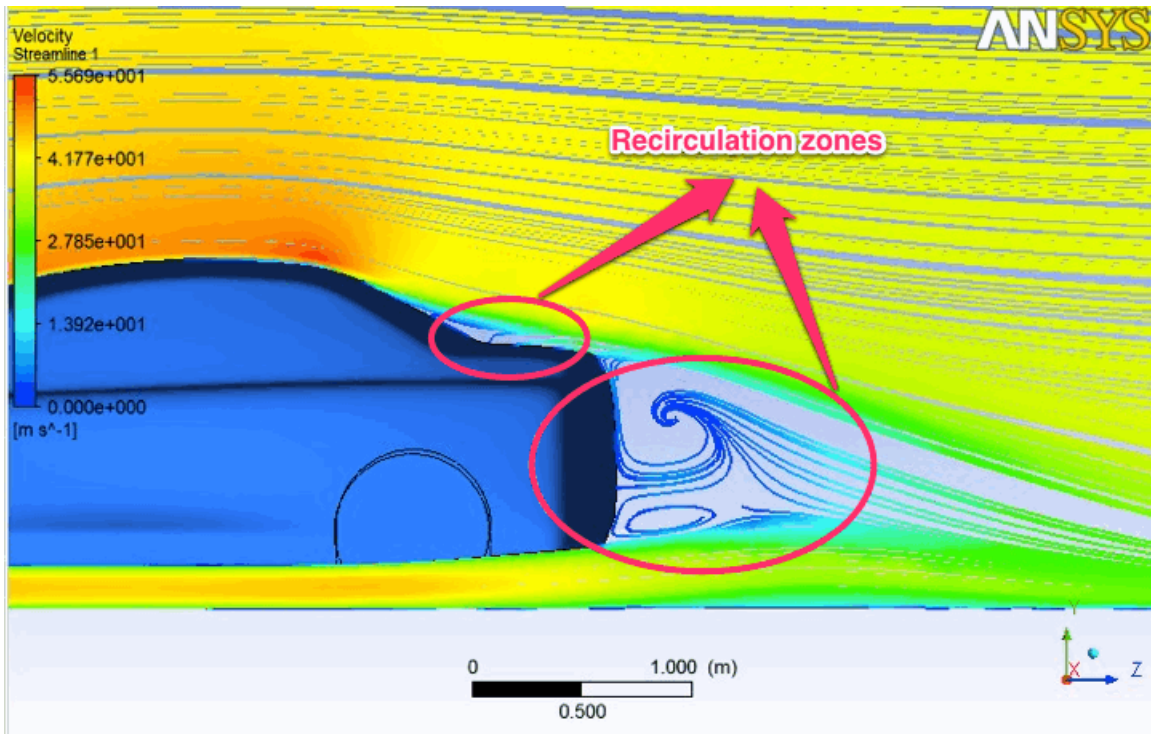


**Figure 5.8** Velocity streamlines of flow in the symmetry plane for case #1

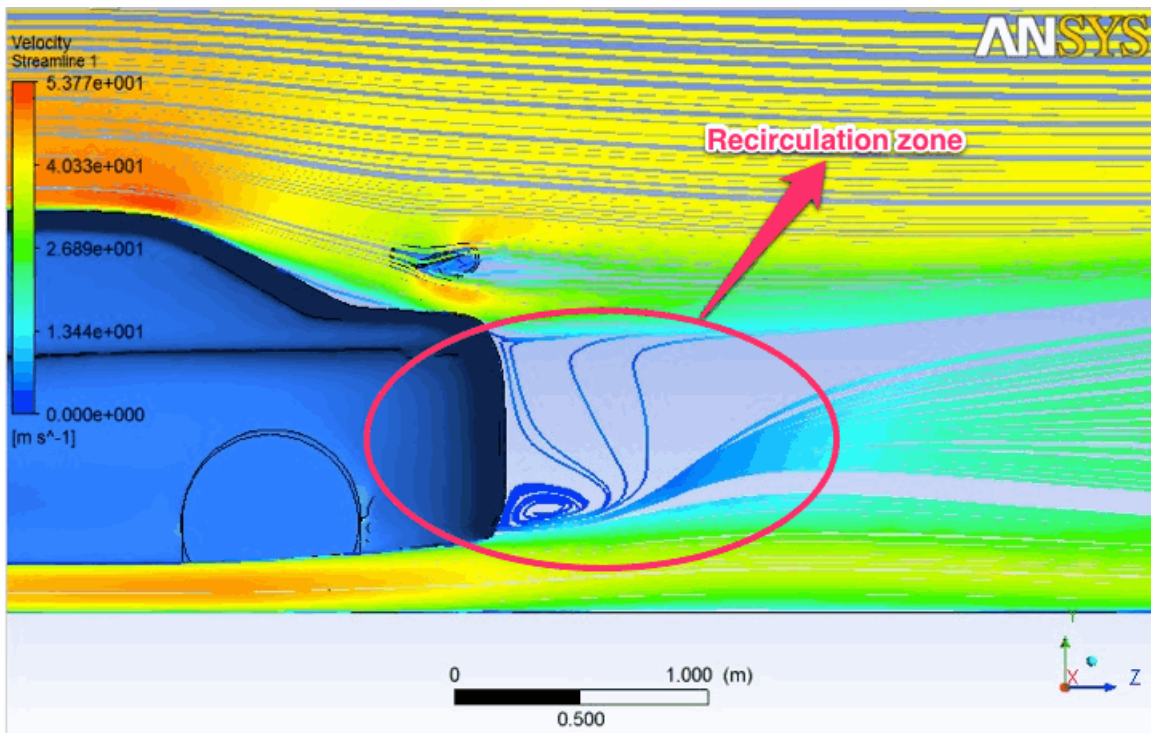


**Figure 5.9** Velocity streamlines of flow in the symmetry plane for case #2



As we see in the **Figure 5.8** there were two different recirculation zones at the rear end of the vehicle (one behind the vehicle, and one above the rear window). By comparing **Figure 5.8** and **Figure 5.9** it has been seen that; the recirculation zone above the rear window was almost gone by using spoiler. The air slopes gently above the rear window, which helps keeping the rear window cleaner. It has been found that keeping the rear window cleaner is one of the advantages of using spoiler.

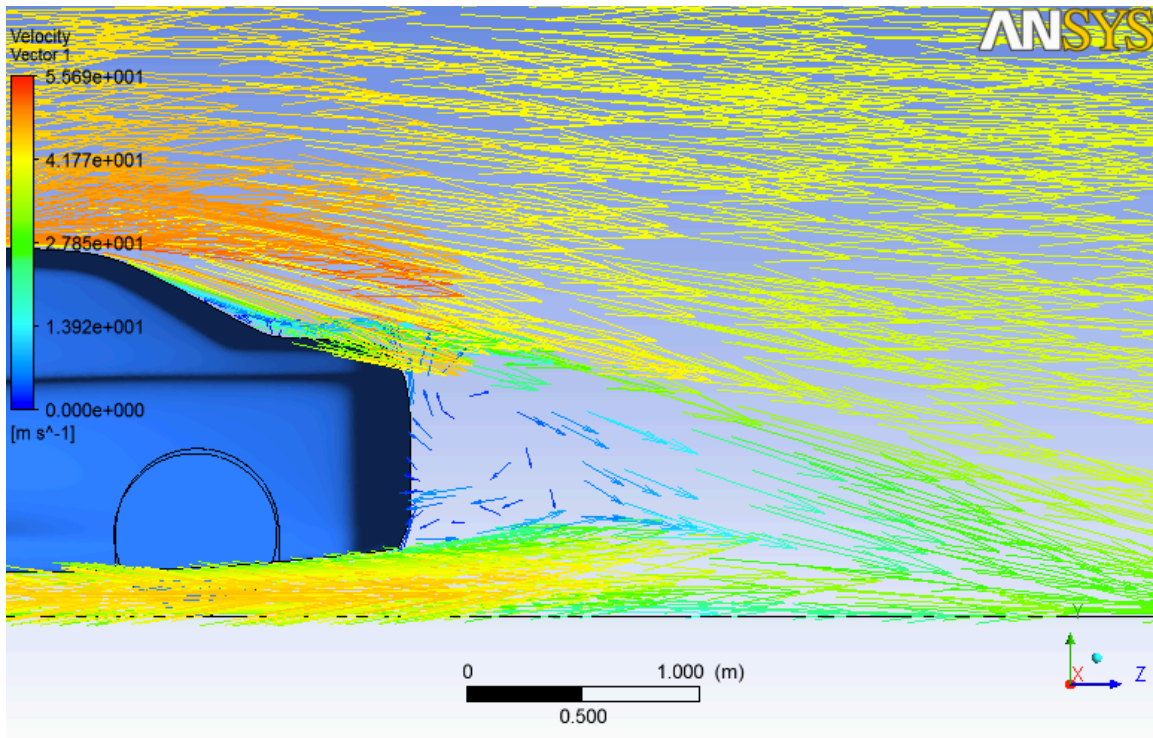


**Figure 5.10** Velocity vectors of flow in the symmetry plane for case #1

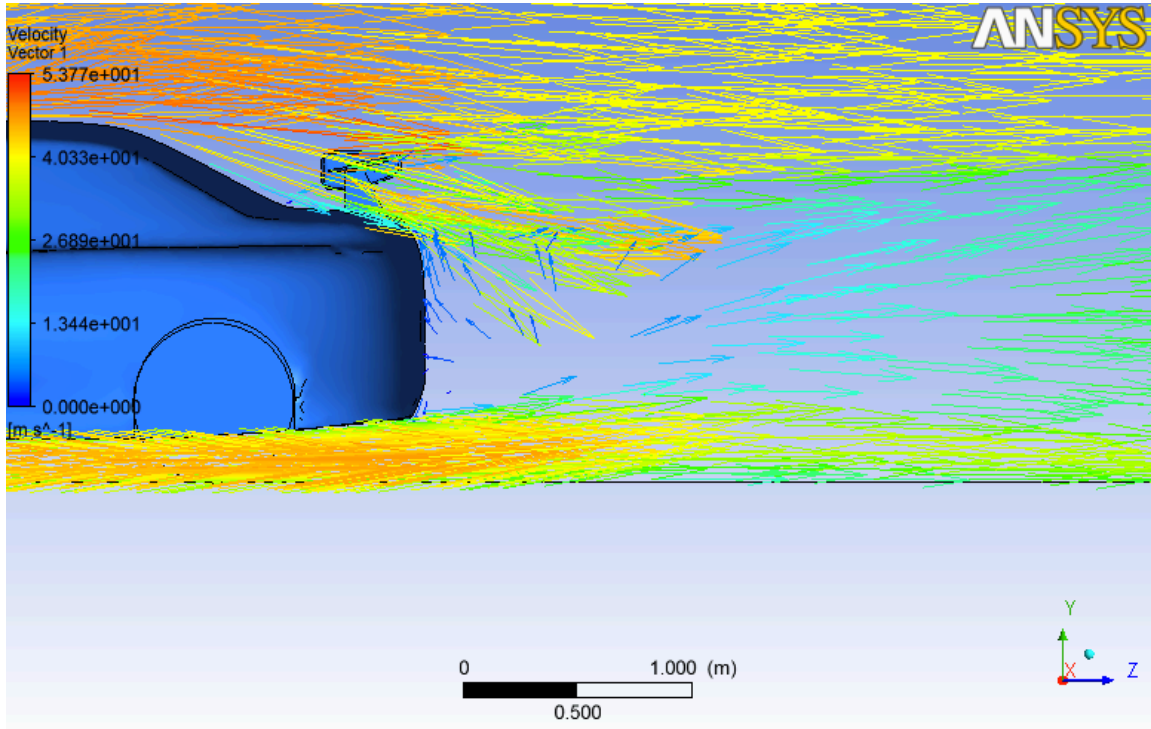


**Figure 5.11 Velocity vectors of flow in the symmetry plane for case #2**

By comparing velocity vectors and velocity streamlines of with/without spoiler situations; (*Figure 5.8, Figure 5.9, Figure 5.10* and *Figure 5.11*) it has been seen that the recirculation zone behind the rear end of vehicle with spoiler is clearly larger.

## **5.2 SIMULATION RESULTS OF BENCHMARK #1, BENCHMARK #2 AND BENCHMARK #3**

The benchmark #1 and benchmark #2 have been performed to understand the differences between fine resolution grids and coarse resolution grids while benchmark #3 has been performed to compare the results of using different turbulence models. For this purpose, the case#2 and its geometry, its convergence history and its simulation results were taken as reference points for all benchmarks and the results were compared based on taking the case #2 as reference point. The solver settings, viscous model and the turbulence model settings that were used for benchmark #1, benchmark #2 and

benchmark #3 have been declared in *Table 4-b* and *Table 4-c* and mesh sizing settings has been declared in the *Table 4-a* previously.

### 5.2.1 BENCHMARK #1: EXAMINE GRID CONVERGENCE

By following the mesh sizing settings that were declared in the *Table 4-a* (which were actually the default settings in ANSYS Meshing®) the mesh we got is shown in *Figure 5.12*.

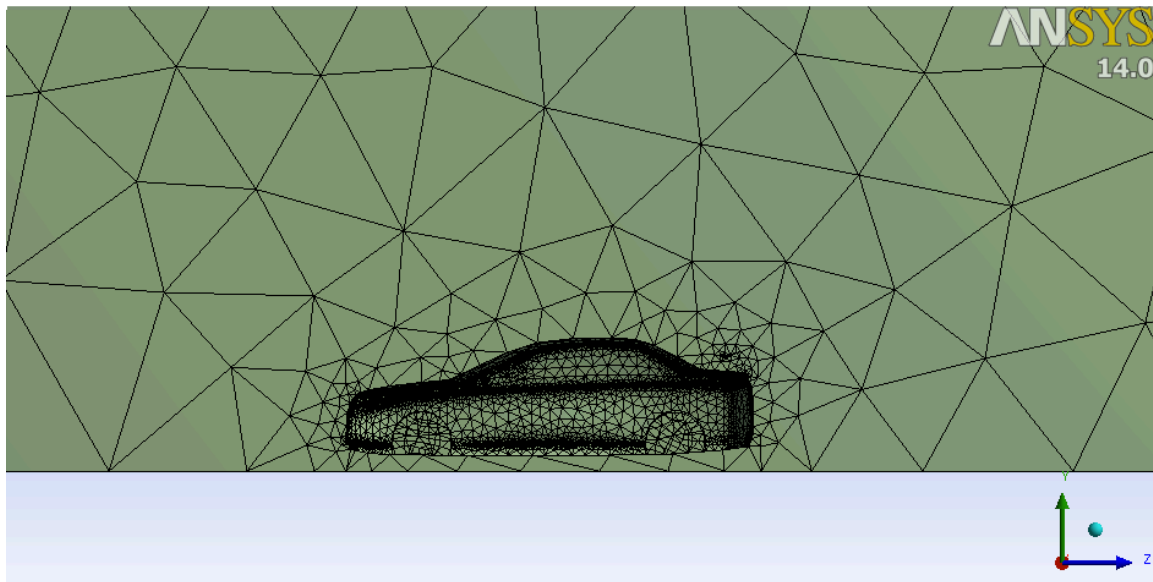


**Figure 5.12** The coarse mesh that used in benchmark #1

After creating the coarse mesh, the next to do is to proceed straight forward to ANSYS FLUENT® Solver setup. The solver settings in the *Table 4-b* were used. Since the meshing is very coarse, 340 iterations took only less than half an hour, while 350 iterations in case #1, case #2 and case #3 took more than 4-5 hours. The criteria to converge were the same, which were having all residuals below  $1e-3$ . The same procedure has been followed which was starting the calculation with first order upwind for the first 100 iterations and switching to second order upwind scheme until it converged. It has been found that, the  $C_D$  and  $C_L$  is almost the same in 100<sup>th</sup> iteration (which was when the scheme was changed to second order upwind) and in 340<sup>th</sup> iteration (which was when the solution was converged with second order upwind). *Figure 5.13*

shows the scaled residual convergence history of benchmark #1 while **Figure 5.14** and **Figure 5.15** shows the drag coefficient and lift coefficient convergence histories respectively.

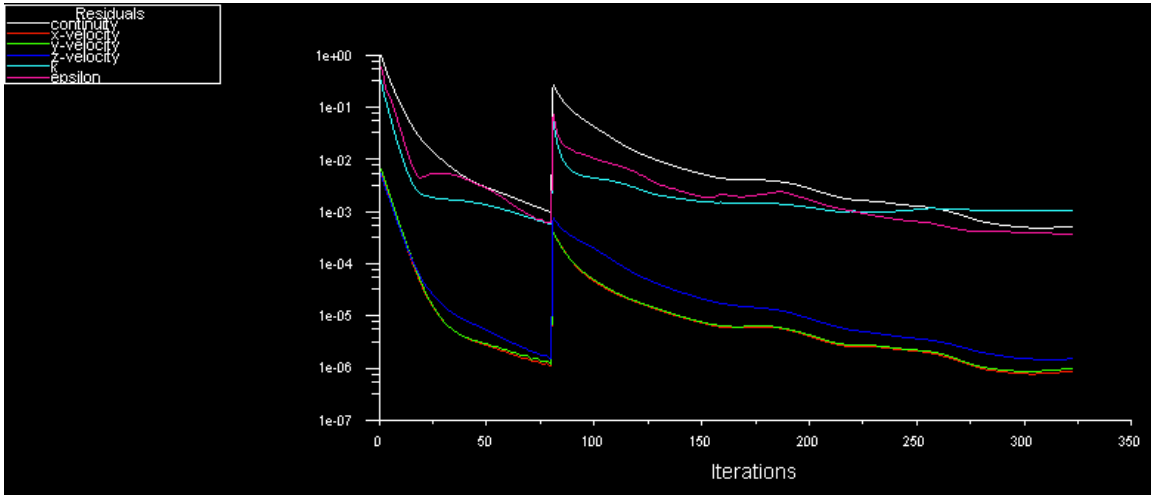


**Figure 5.13** Scaled residuals convergence history of benchmark #1

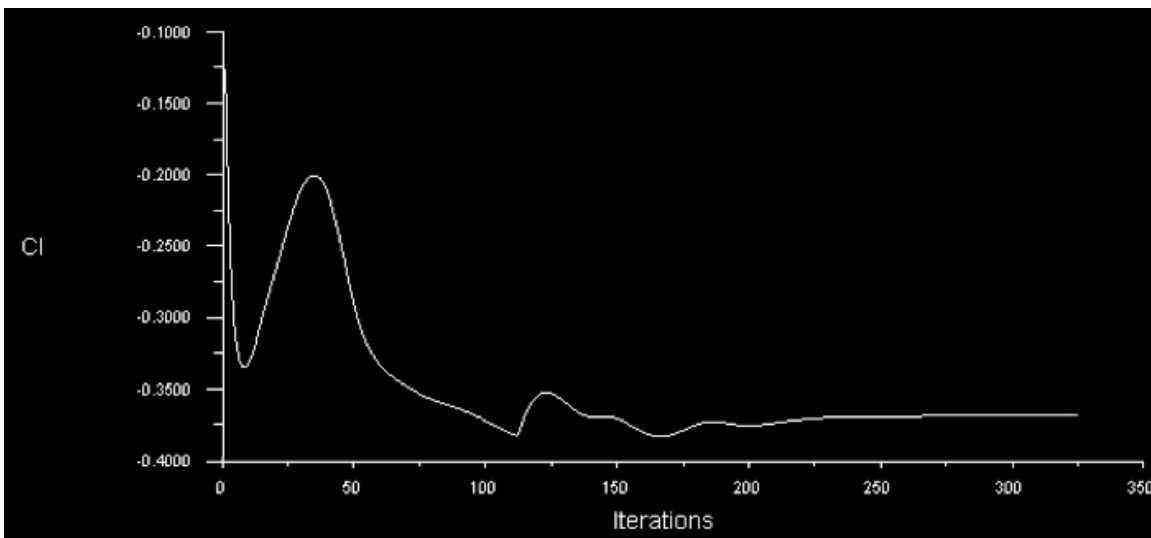


**Figure 5.14**  $C_L$  convergence history of benchmark #1

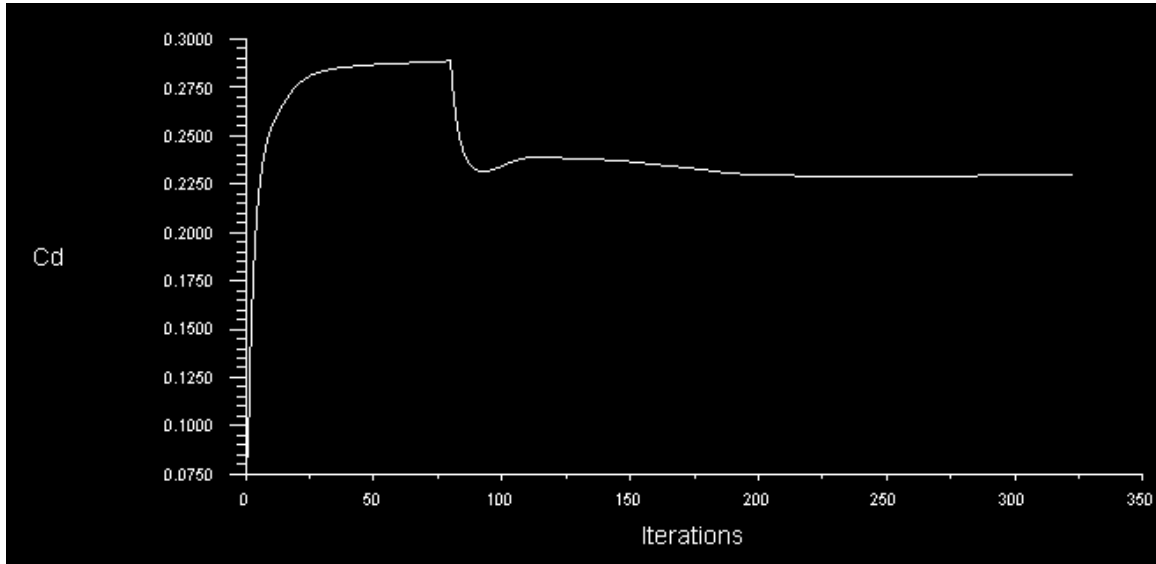


**Figure 5.15  $C_D$  convergence history of benchmark #1**

The calculated  $C_D$  and  $C_L$  were 0.229 and -0.368. The  $C_D$  was close (only 12% difference) to what we have calculated in case #2 but the  $C_L$  was way different (35% difference). If we rebuild the **Table 5-a** by adding the benchmark #1 results, the table would become as seen in **Table 5-b**.

Model	$C_D$	$C_L$
<b>Case #1</b> <i>(Vehicle only + Fine meshing)</i>	0.232	-0.222
<b>Case #2</b> <i>(Vehicle + First spoiler + Fine meshing)</i>	0.192	-0.239
<b>Case #3</b> <i>(Vehicle + Second spoiler + Fine meshing)</i>	0.217	-0.268
<b>Benchmark #1</b> <i>(Vehicle + First spoiler + Coarse meshing)</i>	0.229	-0.368

**Table 5-b Drag and list coefficients for 3 cases + benchmark #1**

### 5.2.2 BENCHMARK #2: EXAMINE GRID CONVERGENCE

The drag and lift coefficients that we have found in benchmark #1 were relatively different than what we have found through case #2, for better understanding the difference between coarse and fine meshing, a new benchmark should have been performed with using medium resolution meshing. In benchmark #2 medium resolution meshing has been used and also the program controlled inflation layers has been applied. We were expecting to get relatively close drag and lift coefficients values in this benchmark #2. By following the mesh sizing settings for benchmark #2 that were declared in the *Table 4-a* the mesh we got is shown in *Figure 5.16*

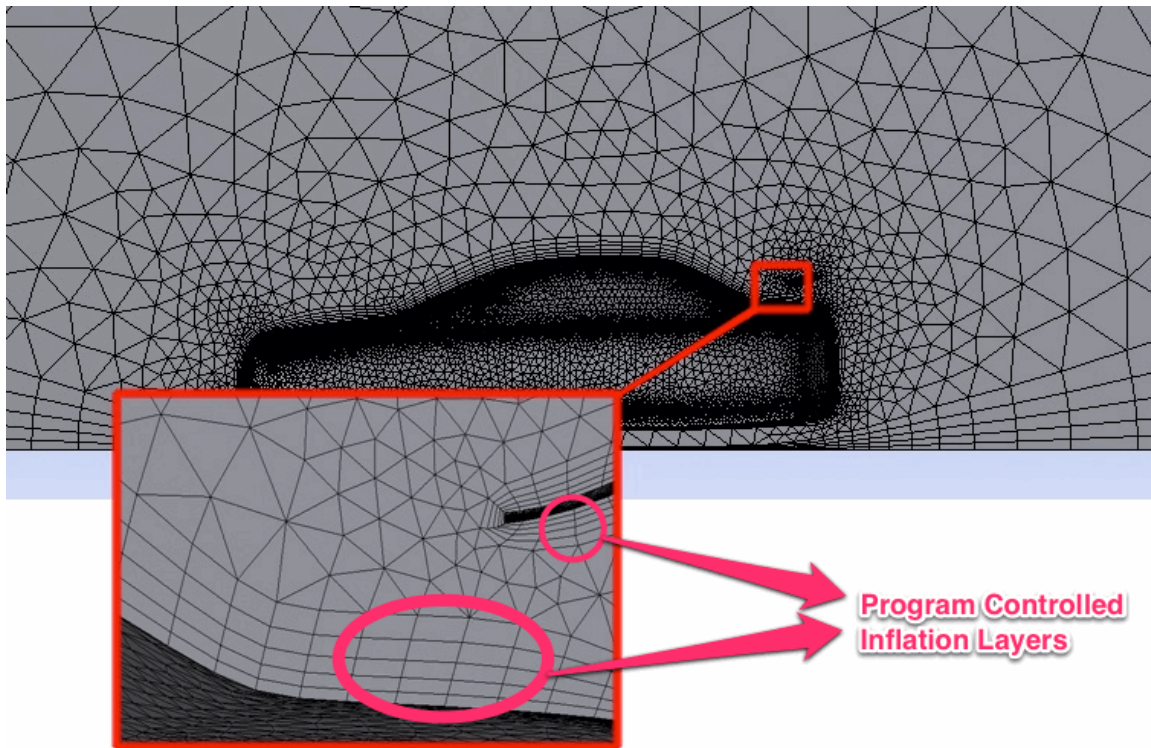


*Figure 5.16* The medium mesh that used in benchmark #2

After creating the mesh, the next to do was to proceed straight forward to ANSYS FLUENT<sup>®</sup> Solver setup. The solver settings in the *Table 4-b* were used. The criteria to converge remained the same, which were having all residuals below  $1e-3$ . And the same procedure has been followed which was starting the calculation for the first 100 iterations

with first order upwind and then continuing until it converged with second order upwind. **Figure 5.17** shows the scaled residual convergence history of benchmark #2 and **Figure 5.18** and **Figure 5.19** show the drag coefficient and lift coefficient convergence histories respectively.

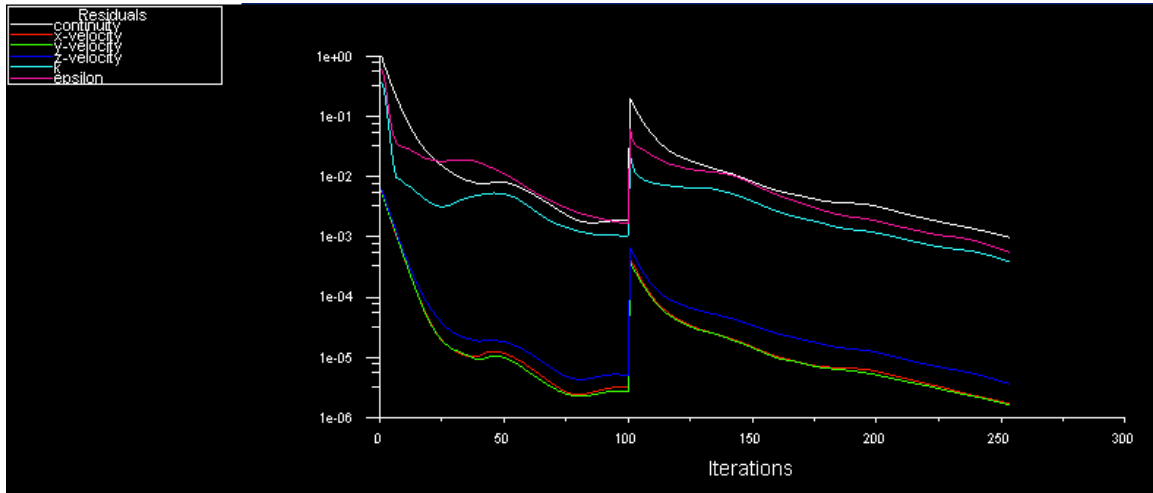


**Figure 5.17** Scaled residuals convergence history of benchmark #2

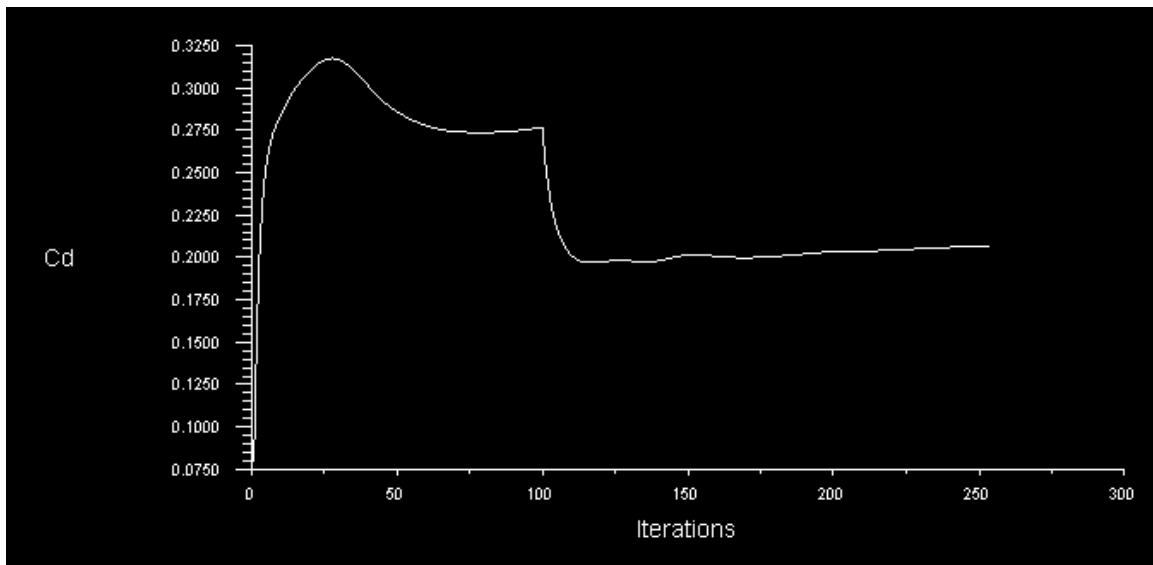


**Figure 5.18**  $C_D$  convergence history of benchmark #2

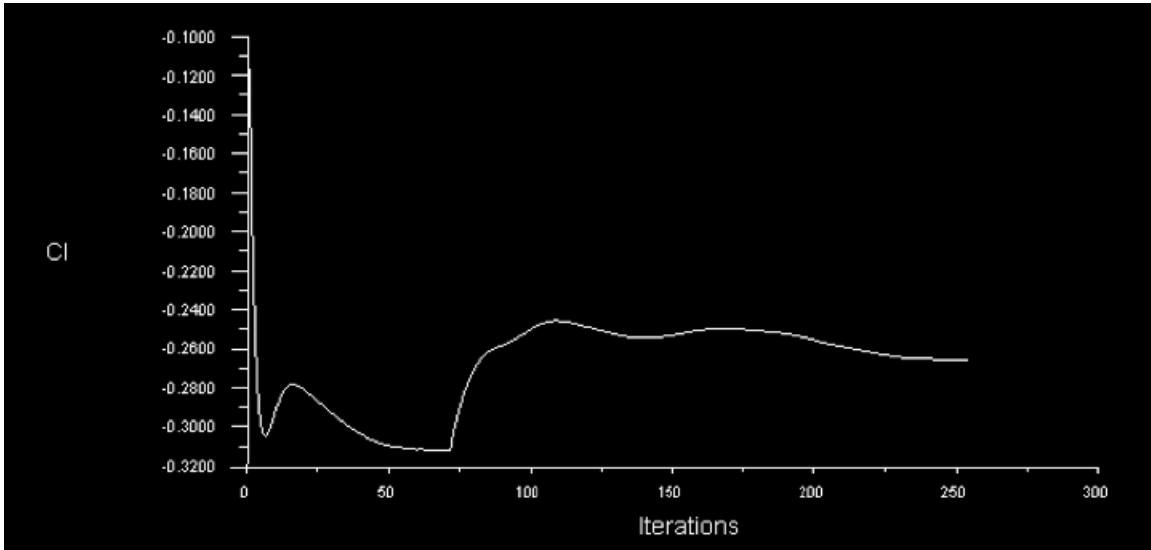


**Figure 5.19**  $C_L$  convergence history of benchmark #2

The calculated  $C_D$  and  $C_L$  are 0.206 and -0.266. The  $C_D$  was only 6% different while the  $C_L$  was only 10% different than what we have calculated in case #2. It has been found by performing benchmark #2 that, higher meshing resolution leads to get more accurate results. If we rebuild the **Table 5-b** by adding the benchmark #2 results, the table would become as seen in **Table 5-c**.

Model	$C_D$	$C_L$
<b>Case #1</b> (Vehicle only)	0.232	-0.222
<b>Case #2</b> (Vehicle + First spoiler + Fine meshing)	0.192	-0.239
<b>Case #3</b> (Vehicle + Second spoiler + Fine meshing)	0.217	-0.268
<b>Benchmark #1</b> (Vehicle + First spoiler + Coarse meshing)	0.229	-0.368
<b>Benchmark #2</b> (Vehicle + First spoiler + Medium meshing)	0.206	-0.266

**Table 5-c** Drag and lift coefficients for 3 cases + benchmark #1 + benchmark #2



### 5.2.3 BENCHMARK #3: EXAMINE MODEL UNCERTAINTIES

The uncertainty in the turbulence models can be examined by running a number of simulations with the various turbulence models and examines the affect on the results. The benchmark #3 has been performed for comparing the results of using different turbulence models. For this purpose, the case #2 and its geometry, its meshing settings were carried exactly the same but the turbulence models were changed to  $k-\omega$ . The new settings for turbulence models and solver settings that used in benchmark #3 have been declared in **Table 4-b** and **Table 4-c**. The results would be compared with what we have gotten from case #2. And also the **Table 5-c** was recreated by adding the new  $C_D$  and  $C_L$  values that we got from benchmark #3 for better understanding the difference. Since we didn't touch the meshing settings at all, the mesh that we are going to use would be same as **Figure 4.12**. *(Only this time it includes the spoiler at the rear end since case #2 that we are going to take as reference, is model of vehicle with the first spoiler)*

The same procedure has been followed. The solution has started with first order upwind for the first 100 iterations to accelerate the convergence and then continued with second order upwind scheme. But  $k-\omega$  turbulence model refused to converge. The “continuity” residual was  $4.83e-3$  at the 280<sup>th</sup> iteration and it went up and down little bit but it became  $4.81e-3$  at 345<sup>th</sup> and 415<sup>th</sup> iterations then even it became  $5.19e-3$  at 430<sup>th</sup> iteration. From that point it tended to go up to  $6e-3$ . Which showed us that it would never converge. Having all residuals below  $1e-3$  was our convergence criteria. Also it has been seen that time consumed for each iteration has also increased comparing to  $k-e$  turbulence model. Due to the lack of computer resources and time, the calculation has stopped at 440<sup>th</sup> iteration. The convergence history of residual for benchmark #3 can be seen in **Figure 5.20**.

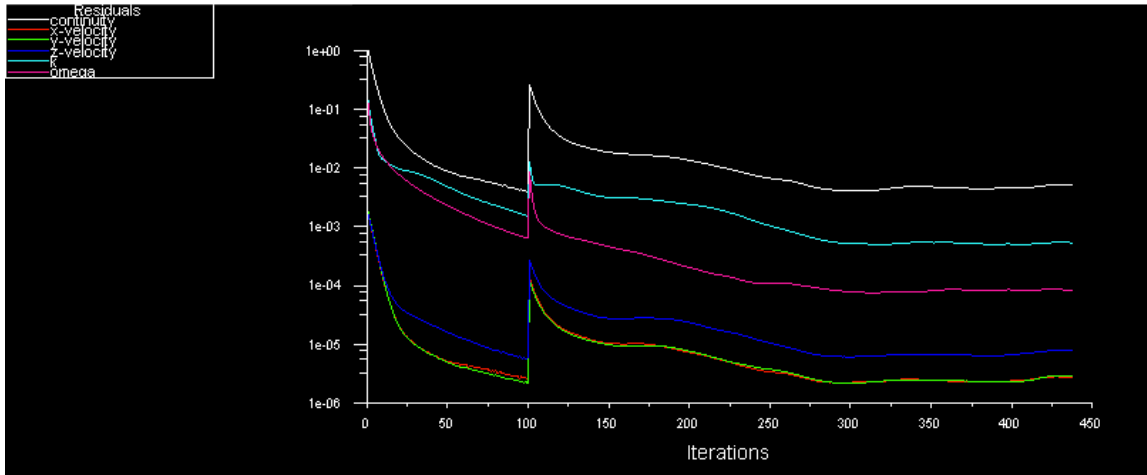


**Figure 5.20** Scaled residuals convergence history of benchmark #3

As it is seen in *Figure 5.21* and *Figure 5.22* the drag coefficient and lift coefficient are still varying. Since the solution refused to converge, and the coefficients tended to change; it was not possible to get a stable drag and lift coefficients.

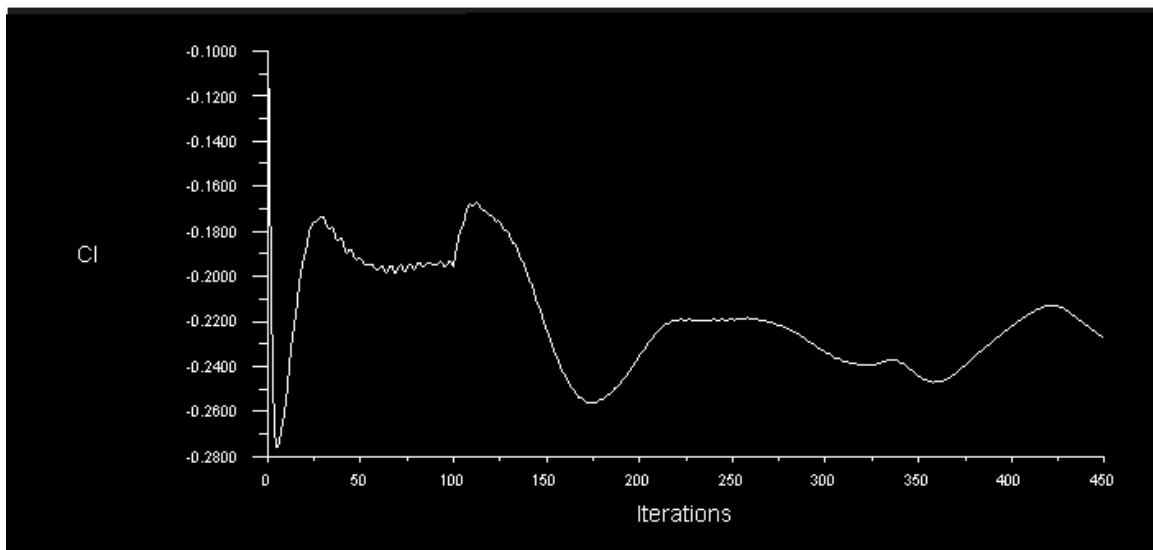


**Figure 5.21**  $C_L$  convergence history of benchmark #3

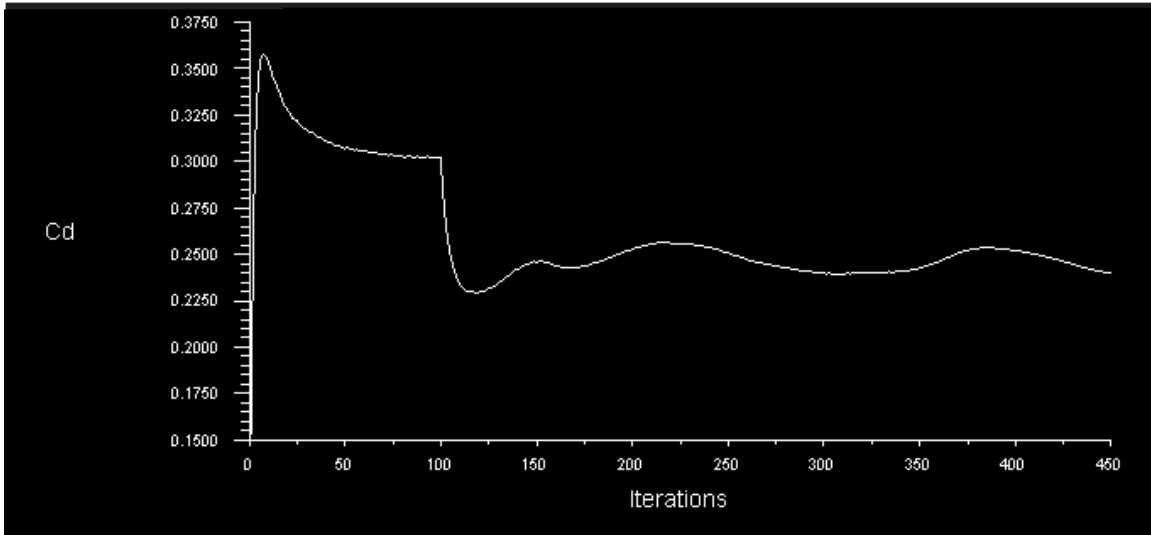


**Figure 5.22  $C_D$  convergence history of benchmark #3**

The calculated  $C_D$  and  $C_L$  at 400<sup>th</sup> iteration were 0.247 and -0.216, which were way different than what we got with the solution from case #2. The solution of benchmark #3 indicates that having a spoiler at the rear end increase the drag and decrease the down-force. Which negatively effects to both forces; then there would be no point to use the spoiler. If we rebuild the *Table 5-c* and add the benchmark #3 results, the table would become as seen in *Table 5-d*

Model	$C_D$	$C_L$
<b>Case #1</b> (Vehicle only + Fine meshing)	0.232	-0.222
<b>Case #2</b> (Vehicle + First spoiler + Fine meshing)	0.192	-0.239
<b>Case #3</b> (Vehicle + Second spoiler + Fine meshing)	0.217	-0.268
<b>Benchmark #1</b> (Vehicle + First spoiler + Coarse meshing)	0.229	-0.368
<b>Benchmark #2</b> (Vehicle + First spoiler + Medium meshing)	0.206	-0.266
<b>Benchmark #3</b> (Vehicle + First spoiler + Fine meshing + $k-\omega$ turbulence model)	0.247	-0.216

**Table 5-d Drag and lift coefficients for 3 cases + benchmark #1 + benchmark #2 + benchmark #3**

## 6 CONCLUSION

The aerodynamic lift, drag and flow characteristics of a high-speed (~65 mph) generic sedan passenger vehicle with a spoiler and without a spoiler situations were numerically investigated. Due to lack of converged solution, time and CPU consuming for each iteration and lack of having constant  $C_D$  and  $C_L$  values; benchmark #3 has showed that the most appropriate turbulence model for external flows around the car body is  $k - \varepsilon$  model. Benchmark #1 and benchmark #2 have showed us that we might face some not appropriate results if the meshing resolution is not fine enough.

Performing benchmark #1 and benchmark #2 have also showed us that higher resolution mesh leads to more accurate results. Drag and lift coefficients that have been obtained through benchmark #2 were closer to case #2 than what have been obtained through benchmark #1. For instance, drag coefficients difference between benchmark #1 and case #2 was 12%, while it was only 6% between benchmark #2 and case #2.

The numerical analyze of high-speed passenger car with first rear spoiler design (case #2, which was a wing style spoiler) has showed that the aerodynamic drag is reduced from 0.232 to 0.192, which is 17% drag reduction, and it also increases negative lift by reducing the lift coefficient from -0.222 to -0.239, which is 7% lift reduction. By comparing *Figure 5.8* and *Figure 5.9* it has been found that; the recirculation zone above the rear window was almost gone by using wing style spoiler (first spoiler). The air sloped gently above the rear window, which helps keeping the rear window cleaner. Numerical analysis has showed us that the second spoiler design (case #1, which was mounted to the edge of rear-end of the vehicle without leaving any gap between spoiler surface and vehicle surface) provided more negative lift force than the first spoiler shape did but provided less drag reduction. It provided 6% drag reduction (dropped the drag coefficient from 0.232 to 0.217) but the negative lift force has been increased by 17% (dropped the lift coefficient from -0.222 to -0.268). It is known that having down force (negative lift force) generates the following advantages:

- ❖ Increases tires capability to produce cornering force
- ❖ Stabilizes vehicles at high speed
- ❖ Improves braking performance
- ❖ Gives better traction

Having more negative force than having less drag can be more important for passenger cars since driving safely is always number one priority. This fact should be kept in mind that; achieving the benefits of a rear spoiler are usually only realized at high speeds. In most cases, a spoiler may actually negatively impact the performance of a car, usually at low speeds. Automobile industry have been working on these side effects and companies have come up with some solutions to eliminate the negative effects of spoiler

in low driving speeds, more about these researches and examples will be discussed in the next chapter, which is “future works”. It is a known fact that every time spoiler generates down force it tends to generate drag. Very high performance sports cars, like Le Mans or F1, have a ratio called the “lift/drag ratio”. The car designers have been trying and maximizing this so that the car has just enough force to get around the corners, but not so much that they are too slow. Indy cars, and ones that are designed like that can have down force in the order of 3G's, at 200mph. That means they could hang completely upside down on the track, and as long as they kept going fast enough, they would still stick to the road.

## **7 FUTURE WORKS**

Companies such as Porsche, Bugatti or Mercedes have been using different technologies for spoilers and trying to maximizing the efficiency of it by eliminating the side effects in low speeds and increasing the advantages on high speeds. One of the most commonly used features is to have a hydraulic wing style spoiler at the rear end of vehicle that raises or lower at certain speeds to maintain down force on the backside of vehicle or to create air brake. This feature has been used mostly for safe driving. Spoiler deployment operation is usually automatic. The software operates the spoiler and fixes it in the certain height depends on the vehicle speed but the driver through a button in the cabin can also operate it. For instance, hydraulic spoiler that has been used in Bugatti Veyron comes up at high speeds to hold the car on the road better by creating down force. When the car reaches 220 km/h (140 mph), small hydraulic spoiler deploys from the rear bodywork and a wing extends about a foot. This configuration produces substantial down force, provides up to 330 pounds in front and 440 in the rear [16], which helps holding the car to the road in extreme speeds.

## LIST OF REFERENCE

1. John J. Bertin, “**Aerodynamics for Engineers**”, Prentice Hall; 5<sup>th</sup> edition, New Jersey, June 2008
2. Jiyuan Tu, Guan Heng Yeoh and Chaoqun Liu, “**Computational Fluid Dynamics: A Practical Approach**”, Butterworth-Heinemann; 1<sup>st</sup> edition, Burlington, MA, November 2007
3. Oleg Zikanov, “**Essential Computational Fluid Dynamics**”, John Wiley & Sons, Inc. Hoboken, New Jersey, March 2010
4. C. H. K. Williamson, “**Three Dimensional Vortex Dynamics in Bluff Body Wakes**”, Experimental Thermal and Fluid Science, Volume 12, February 1996, p. 150-168
5. 1. Wolf-Heinrich Hucho, “**Aerodynamics of Road Vehicles: From Fluid Mechanics to Vehicle Engineering**”, Society of Automotive Engineers Inc; 4<sup>th</sup> edition, Warrendale, Pa, February 1998
6. Website: [http://autospeed.com/cms/title\\_Aero-Testing-Part-4/A\\_108676/article.html](http://autospeed.com/cms/title_Aero-Testing-Part-4/A_108676/article.html)
7. Marco Lanfrit, “**Best practice guidelines for handlingAutomotive External Aerodynamics with FLUENT**”, Fluent Deutschland GmbH, 64295 Darmstadt/Germany, February 2005
8. W. Seibert “**CFD in Aerodynamic Design Process of Road and Race Cars**”, Fluent Deutschland GmbH, FLUENT Technical Notes TN155, Presented at European Automotive Congress, Bratislava, Slovakia, June 18-20 2001
9. Klaus Gersten, E. Krause, H. Jr. Oertel, C. Mayes “**Boundary-Layer Theory**”, Herrmann Schlichting, 8<sup>th</sup> Edition, Springer 2004
10. W. Seibert, M. Lanfrit, B. Hupertz and L. Krüger “**A Best- Practice for High Resolution Aerodynamic Simulation around a Production Car Shape**” 4<sup>th</sup> MIRA International Vehicle Aerodynamics Conference, Warwick, UK, October 16-17, 2002

11. **“FLUENT 6.0 User’s Guide - Volume 1”**, ANSYS Inc., New York, December 2001.
12. **“ANSYS FLUENT 12.0/12.1 in Workbench User's Guide”**, ANSYS Inc., New York, October 2011
13. **“ANSYS FLUENT 12.0 Theory Guide”**, ANSYS Inc., New York, April 2009
14. Masaru KOIKE, Tsunehisa NAGAYOSHI and Naoki HAMAMOTO, **“Research on Aerodynamic Drag Reduction by Vortex Generator”**, Mitsubishi Motors Technical Reviews, Tokyo, Japan, 2004
15. M. Rouméas, P. Gilliéron & A. Kourta **“Drag Reduction by Flow Separation Control on a Car After Body”**, Int. J. Numer. Methods Fluids 60, 2008 . ISSN 0271-2091
16. A. Kourta, P. Gilliéron **"Impact of the Automotive Aerodynamic Control on the Economic Issues"**, Journal of Applied Fluid Mechanics , Vol. 2, No. 2, pp. 69-75, 2009, ISSN 1735-3645
17. Byoung-Kwon Lee, MD **"Computational Fluid Dynamics in Cardiovascular Disease"** Korean Circulation Journal 41(8): 423–430, August, 2011
18. Website: <http://bugattipage.com/ride.htm>
19. Website: <http://www.nasa.gov/audience/forstudents/5-8/features/what-is-aerodynamics-58.html>
20. Website: <http://www.grc.nasa.gov/WWW/K-12/airplane/boundlay.html>